



UNIVERSIDAD NACIONAL AUTÓNOMA DE MÉXICO
DOCTORADO EN CIENCIAS (FÍSICA)
INSTITUTO DE CIENCIAS FÍSICAS

COMB-LIKE TURING PATTERNS EMBEDDED IN HOPF OSCILLATIONS

TESIS
QUE PARA OPTAR POR EL GRADO DE:
DOCTOR EN CIENCIAS (FÍSICA)

PRESENTA:
PAULINO MONROY CASTILLERO

COMITÉ TUTOR:

Dr. FRANCOIS ALAIN LEYVRAZ WALTZ
INSTITUTO DE CIENCIAS FÍSICAS, UNAM

Dr. THOMAS HENRY SELIGMAN SCHURCH
INSTITUTO DE CIENCIAS FÍSICAS, UNAM

Dr. THOMAS GORIN
DEPARTAMENTO DE FÍSICA, CUCEI, UdeG

CUERNAVACA, MOR., OCTUBRE 2017



Universidad Nacional
Autónoma de México

Dirección General de Bibliotecas de la UNAM

Biblioteca Central



UNAM – Dirección General de Bibliotecas
Tesis Digitales
Restricciones de uso

DERECHOS RESERVADOS ©
PROHIBIDA SU REPRODUCCIÓN TOTAL O PARCIAL

Todo el material contenido en esta tesis esta protegido por la Ley Federal del Derecho de Autor (LFDA) de los Estados Unidos Mexicanos (México).

El uso de imágenes, fragmentos de videos, y demás material que sea objeto de protección de los derechos de autor, será exclusivamente para fines educativos e informativos y deberá citar la fuente donde la obtuvo mencionando el autor o autores. Cualquier uso distinto como el lucro, reproducción, edición o modificación, será perseguido y sancionado por el respectivo titular de los Derechos de Autor.

Dedicada a mis padres.

Por las siguientes aventuras en que nos embarcaremos.

Agradecimientos

Son muchas las personas, actores e instituciones a quien agradecer en toda esta etapa dentro del posgrado en física; es por ello que la probabilidad de que involuntariamente omita a alguno es alta. Empezaré a mencionar lo institucional, y después todo lo demás.

Agradecimiento a la Coordinación de Estudios de Posgrado de la UNAM, que me dio la beca de manutención por año y medio y me permitió el ingreso de tiempo completo al programa de maestría en el Posgrado en Ciencias Físicas (PCF). Al PCF y, en particular, a Rafael Pérez Pascual por orientarme y estar pendiente de mi caso tanto para el ingreso al programa de maestría como al de doctorado. Al Instituto de Ciencias Físicas (ICF), tanto administrativos, trabajadores, profesores y estudiantes por brindar una agradable disposición y hacer lo posible para que las cosas salgan adelante. A CONACYT por el soporte con la beca de manutención a lo largo de cuatro años, por los recursos del PNPC y del proyecto CONACYT No. 219993; a la UNAM por los recursos de proyectos DGAPA-PAPIIT IN100616 y IN103017, así como como PAEP en distintos años. Dichos recursos contribuyeron significativamente a mi formación personal y al desarrollo particular de la colaboración internacional y la publicación del artículo producto del trabajo de investigación que se presenta en esta tesis.

Agradezco fuertemente a todos mis tutores. Tuve la fortuna de tener cinco tutores, tres oficiales y dos putativos, y no fue por algún esquema administrativo vano o circunstancia eventual, sino porque me tocó hacer trabajo fuerte con cada uno y también una amplia convivencia y cercanía; así pude aprender muchas cosas de ellos. De cada uno albergo una gran admiración y estima. Como primer agradecimiento personal menciono a Thomas H. Seligman, quien desde el día que nos conocimos, tan sólo por un entendido de palabra procuró generarme las condiciones para integrarme al grupo de investigación y de ahí en adelante año tras año me ha ido abriendo puertas para fortalecerme y hacer cosas con mayor alcance, gracias por todo el soporte y la confianza depositada en mí. Con Thomas pude ver formas amplias de entender un ejercicio profesional y a la vez personal para la conformación sólida de un grupo, lo que antes tan sólo me lo podía imaginar vagamente. Mi siguiente agradecimiento es para Arik Yochelis, quien me mostró un campo amplio y desconocido para mí en el ámbito de las matemáticas: ecuaciones de reacción-difusión y formación de patrones. Fue durante una estancia con Arik en la Universidad Ben-Gurion del Negev, en un campus en medio del desierto, donde surgió el presente tema de investigación. De ahí en adelante trabajamos en conjunto por dos años y medio en este proyecto hasta que se publicó el artículo. Arik ha resultado para mí un verdadero ejemplo de profesionalismo, disposición y buena voluntad en cada aspecto en que convivimos. Continuando, mi gran agradecimiento para Francois A. Leyvraz, una persona impresionante con quien espero tener muchas más charlas, discusiones o proyectos. Somos afortunados todos los del instituto de tener a alguien así de fuerte y que sea tan cercano y accesible para dedicarnos tiempo de manera holgada. Particularmente gracias Francois por la paciencia y el apoyo en todo momento, que me ayudó a resolver los aspectos técnicos y pesados de este trabajo. Doy un gran agradecimiento a Abraham Jalbout por las oportunidades que me otorgó, por su amistad, por todo lo que generamos en conjunto y porque me abrió un panorama mucho más amplio del que yo había visualizado anteriormente, además de las variadas aventuras académico-productivas en las que nos zambullimos. Por último agradezco a Thomas Gorin, ejemplar persona tanto en lo personal como en lo profesional, agradezco por

todo el respaldo que me dio y disposición para hacer avanzar cada cosa en donde concurrimos; admiro su audacia y su filo de pensamiento que nos llevó a plantear uno de los problemas que más me emocionan actualmente y que es un buen jugo que le hemos sacado a tantas búsquedas y reflexiones.

También agradezco a los distintos profesores con quienes tuve estancias o que fueron importantes para perfilar buen rumbo y aprendizajes: Itamar Procaccia, Tomaz Prosen, Thomas Guhr, Rudi Schaefer, Ruben Fossion, Hernán Larralde, Markus Mueller, Carlos Pineda, Rafael Pérez Pascual.

A Carlos, Héctor, Mayra, Diana P., Braulio, Susana, Arturo y David por la compañía, los planes y complicidades que tramamos o que en efecto llevamos a cabo. A Hans y a Lore porque me metieron fuerte en la carrera con su tesón y su amistad. Gracias a Omar A. y Andrés L. por hacer las cosas codo con codo. A Jaz y Yorch por la familia que hicimos. A Vinayak por guiarme y darme confianza para avanzar. A Juan e Iván por el gran equipo que logramos en Hermosillo. A Kary y Laura C. por su soporte tan grande que me ha permitido seguir este año. A Gil, Pablo, Chuy y Marcelino que siempre me extienden la mano y en esta etapa estuvieron presentes en momentos clave. A R. M. por instruirme en la forma de razonar, por empujarme a hacerme más fuerte y por ser un aliado macizo. A J. R. por ser nakama y no dejarme perder de vista que la afinidad puede llevar a cosas eminentes y con un sentido propio.

A mis papás por apoyarme con los aspectos más fuertes y en los momentos cruciales. A Gerardo y Rosa Elena por seguir siendo compañeros en cosas reales aún con la distancia. Y en general a toda la familia Monroy y a la Castillero que desde sus trincheras me han apoyado en distinto tiempo y maneras. También agradezco al equipo techero que por años siguió trabajando mientras que yo sólo quedé de espectador después de mi partida.

En general, a todxs lxs involucradxs que, voluntaria o involuntariamente, hicieron que mi estancia en Cuernavaca y CDMX haya resultado agradable y significativa. A todo el ámbito deportivo generado con Nápoles, C. Físicas, Necaxa, UNAM campus Morelos, Física, Barbas, Mambas, Zombies, Radicales, Panteras, etc. Gracias a Braulio, Adri, Yoab, Jaz y Remi por ser eslabones fuertes para vivir cotidianamente esto. También todo lo hecho y generado alrededor de la música, gracias a Abraham T. y lo vivido con Jóvenes, a mis adoradxs amigxs Cenzontles, a Mara y Felipe que me dieron peldaños para avanzar en mis pretensiones.

Y, especialmente, gracias a Nadia, Diana G., Omar, Karina, Marian, Ángel, Diana D. y Yoab, por quienes sé con claridad que han valido la pena estos años aquí: con ustedes he podido engarzar cosas valiosas nada triviales, formar una unidad entrañable y vivir escenarios que antes sólo soñaba.

Descripción general de la contribución del trabajo

En este trabajo es presentado el proyecto de investigación desarrollado en colaboración con el Dr. Arik Yochelis de la Universidad Ben-Gurion de Israel, cuyos resultados fueron publicados en abril del presente año en la revista *Chaos* (<http://aip.scitation.org/doi/10.1063/1.4981394>).

El trabajo muestra un mecanismo genérico para la formación de estados localizados en el espacio, inmersos en un entorno oscilatorio en el tiempo. En el marco de un sistema no lineal oscilatorio forzado con acomplamiento de frecuencia 2:1. La localización de estos estados es del modo Turing, en un dominio espacial bidimensional y tiene una forma de *peine*. Puede verse tanto en el la region intermedia de un frente de oscilaciones de Hopf, divididas por un desplazamiento de π en la phase, o también puede verse en el centro de espirales de Hopf. Específicamente, los estados localizados aparecen en un rango de parámetros más amplio en donde no se sostiene la dinámica *flip-flop* que es muy conocida que ocurre dominios espaciales de una sola dimensión y en una vecindad de la bifurcation Hopf-Turing.

Se realizó tanto análisis lineal como análisis no-lineal débil para obtener resultados analíticos respecto a la amplitud de los modos Hopf y Turing, tomando en cuenta dos direcciones perpendiculares del modo Turing. Con las ecuaciones de amplitud se realizó trabajo analítico como numérico. El trabajo muestra cómo el frente de Hopf rompe la simetría y propicia la formación de estados localizados de Turing en dirección perpendicular al frente.

Los resultados obtenidos concuerdan, dentro de los márgenes de precisión, con que la dinámica del modo Turing perpendicular al frente de Hopf es el mismo mecanismo que permite la existencia de los estados localizados dentro de espirales de Hopf. Dentro del contexto de resonancia no lineal 2:1, estos resultados muestran que existe una region más amplia donde se pueden encontrar estados con resonancia, aunque no en todo el dominio sino en una región localizada. Esto lleva a implicaciones particulares que ya han sido vistas en reacciones químicas tipo Belousov-Zhabotinsky y medio granular.



Asunto: Aceptación de tesis escrita en idioma inglés

MONROY CASTILLERO PAULINO
ALUMNO DE DOCTORADO EN CIENCIAS (FÍSICA)
NÚMERO DE CUENTA: 511013621

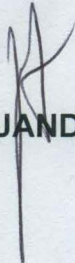
PRESENTE

Por este conducto me permito informarle que el Comité Académico del Posgrado en Ciencias Físicas en su sesión del **2 de mayo** del presente, aprobó su solicitud para escribir su trabajo de tesis de maestría en idioma inglés, teniendo como requisito incluir en la tesis un resumen extenso en español.

Sin otro particular, reciban un cordial saludo.

ATENTAMENTE
“POR MI RAZA HABLARÁ EL ESPÍRITU”
Ciudad Universitaria, Cd. Mx., a 8 de Mayo de 2017.
EL COORDINADOR DEL POSGRADO EN CIENCIAS FÍSICAS

DR. JORGE ALEJANDRO REYES ESQUEDA
c.c.p. Expediente



Contents

1	Introduction	11
1.1	Thesis structure	11
1.2	Research work abstract	12
2	Preliminaries	13
2.1	Pattern formation overview	13
	Natural phenomena	13
	Reaction-diffusion equations	15
	Stationary and oscillatory instabilities	16
	Experimental realization of pattern formation	19
2.2	Pattern formation analysis	20
	Instabilities generated by diffusion	20
	Dispersion relations and growth rate curves.	23
	Non-uniform stationary instability	25
	Uniform oscillatory instability	27
	Weak non-linear analysis: Amplitude equations	29
	Amplitude equations for uniform oscillations	33
	Frequency locking	37
	1D localized patterns and homoclinic snaking	38
2.3	Previous research in the field	40
	Coexistence of periodic stationary and temporal patterns: Hopf-Turing bifurcation	40
	Frequency locking outside the resonant region	40
	Flip-flop dynamics, depinning and homoclinic snaking	43
3	Research work	47
3.1	Comb-like patterns and its parameter region	48
3.2	Comb-like localized states	49
	Weakly nonlinear analysis	51
	Stability and Hopf fronts	52
	Numerical results	54
3.3	Spiral waves with comb-like core	56
3.4	Conclusions	56

4 Appendix	59
.1 Multiple scales and weakly non-linear analysis	59
.2 Solvability conditions	65
.3 Useful identities and some algebra simplifications	68
Bibliography	69

Chapter 1

Introduction

1.1 Thesis structure

This thesis work is conformed by three main sections: the preliminaries, the research work, and the appendix.

The objective of chapter “*Preliminaries*” is to provide a glimpse of the pattern formation as a field of research, to give introduction and intuition of the mathematical framework used on it and to present the previous work that preceded our research project. The first part is about pattern formation phenomena: natural appearance, our understanding of the phenomena through dynamical systems, reaction-diffusion equations and the different types of instabilities; and some experimental realizations. Then the section focuses in introducing the mathematical methods commonly used in this area, and also we will show important results that are the backbone of this study (for example, the amplitude equation for a periodically forced system with a Hopf instability, called the Forced Complex Ginzburg Landau (FCGL) equation). At the end of the chapter we will show some of the previous research that was important to frame this research project. As the objective of this part is not the production of didactic material, but only to present the field in general and to present the theoretical framework that is used in the research work, I will simply use the same way to introduce the concepts and topics as some of the references do. The structure of this chapter and also many of the particular examples and the general scope of the topic were mainly based on the book of Ehud Meron, *Nonlinear physics of ecosystems* [[Mer15](#)].

In the research work chapter, we present the results of our research project, which also have been recently published [[MCY17](#)]. First we talk about some characteristics of the region at the border of the resonance tongue, and specify the parameter region where the comb-like Turing pattern appears. Then we explain why this particular Hopf-Turing coexistence is of a different nature than the 1D case (flip-flop). Amplitude equations near the codimension-2 Hopf-Turing instability, with Hopf and two perpendicular Turing modes are presented. It is shown how a Hopf front breaks the symmetry of the perpendicular Turing modes and it is possible to identify their different interac-

tions. At the end we compared the results taken from amplitude equations, in which we obtained the length domain of the perpendicular mode for different γ , with respect to the length of comb-like patterns that appear in the original system.

In the appendix we present the step by step calculations for the weakly non-linear analysis to obtain the amplitude equations that were a crucial part of the research.

1.2 Research work abstract

Chemical reactions are frequently being used as case models to elucidate generic and rich mechanisms of spatiotemporal dynamics, such as the spatial periodic Turing patterns, spiral wave dynamics, bistability, domain walls, and spot replication [MPC97, KM10, Mur02, KS98] (and the references therein) by providing insights into mathematical mechanisms (e.g., linear, nonlinear, absolute, and convective instabilities) that give rise to pattern selection [CH93, BDDW⁺02, Pis06]. Among the more popular and exploited reactions are Belousov-Zhabotinsky and chlorite-iodide-malonic-acid (CIMA) [ES96, BDDW⁺02]. Besides interests in chemical controls [DKBE90, BDDW⁺02, VE08, SCT⁺12], these reactions are also used as phenomenological models for biological and ecological systems, examples of which include morphogenesis, cardiac arrhythmia, and vegetation in semi-arid regions [CH93, VP09, ES96, Mer15].

An intriguing type of pattern formation phenomenon, demonstrating stationary spatial localization embedded in an oscillatory background, has been found experimentally in the CIMA reaction [DKPBE94]. Such localized states have been observed in one- and two-space dimensions (1D and 2D, respectively) [BJP⁺95, DBDW⁺95], and attributed to a Turing core emerging in a oscillating Hopf background. In 1D the oscillatory background obeyed phase shifts of π , a behavior that is typical in the vicinity of a codimension-2 bifurcation [DKPBE94, JPM⁺94, MHM09], a.k.a. a *flip-flop* behavior or “1D-spiral” [PDWD⁺93, Bha07, DWLDB96]. The 2D localization was attributed to the phase singularity that forces a vanishing Hopf amplitude and thus in turn emergence of a Turing state [DKPBE94, JPM⁺94, MHM09]. In the mathematical context, it was shown that the spatial localization in the 1D Hopf-Turing bifurcation [TMB⁺13, JPM⁺94] bears a similarity to the spatial localization mechanism in systems with a finite wavenumber instability due to the *homoclinic snaking* structure [TMB⁺13].

Chapter 2

Preliminaries

2.1 Pattern formation overview

Natural phenomena

Patterns in nature are visible regularities of form found in the natural world, some examples are shown in Fig. 2.1. These patterns recur in different contexts and can sometimes be modelled mathematically. Natural patterns include symmetries, trees, spirals, meanders, explosions, waves, foams, tessellations, cracks and stripes, among others [Ste15]. Spontaneous pattern formation in nature is an intriguing phenomenon that has kept the attention in different fields, first to understand their underlying mechanisms of formation and then to obtain better means of control to get desired state configurations in the evolution of particular systems.

The general idea given by the principle of macroscopic uniformity is that a system made of a huge number of particles achieves a stationary state when the maximum entropy is reached and, at this point, homogeneous macroscopic characteristics should appear [Ste08]. But patterns and structures found everywhere in nature prove that there are obviously mechanisms that lead to non-homogeneity in stationary states. Diverse mechanisms are the cause for each case, but here we are especially interested in patterns whose particular shapes were not crafted by an external factor directly, but by its own dynamics behavior or, more precisely, the dynamics of its constituents at local scale.

Self-organization is a process where some order or some global structure arise due to local interactions that can start even from a disordered initial state. There exist some systems which exhibit self-organization due to positive feedbacks in its dynamics that lead to the pattern formation that we are interested in. When a system starts from a macroscopically homogeneous state, which has translational symmetry, and evolves into a patterned state, it means that the symmetry was broken at some point, this phenomenon is called a *symmetry breaking instability* [Mer15]. Although it can not be really proven that patterns found in nature come from symmetry breaking instabili-



Figure 2.1: From left to right. A spotted cheetah and a king cheetah patterns [Bon12], cloud stripes [Oel14], vegetation patterns [Wik17] and sand ripples [Bal15].

ties, nowadays there are simulations from mathematical models and also experiments that give a strong confidence in it, and it's a good aspect of the theory that there is no need of a special initial configuration for the emergence of the pattern and it can work with random initial conditions. Certainly, it is thoroughly unlikely to find systems in nature standing in a unstable equilibrium, but it is much more plausible to witness a system in a stable equilibrium that changes until the equilibrium becomes unstable and the breaking of symmetry occurs. In the models, the parameters of the system could change the condition of a stable equilibrium into an unstable one; when there is a parameter λ that can make this change it is called the *control parameter*, when the control parameter reaches a certain threshold λ_c , then the equilibrium goes from stable to unstable. It is called a *bifurcation* when this stability characteristic changes and occurs when $\lambda = \lambda_c$ [CH93].

Alan Turing submitted in 1951 an article in which he intended to explain morphogenesis (the biological process that generates the shape of an organism, from a spherically symmetric blastula to an embryo) based on the chemical reactions of substances that could occur in the blastula [Tur52]. Obviously, the blastula is spherically symmetric only in a macroscopic point of view, but it has small fluctuations that make possible an unsymmetrical further evolution. Citing Turing's paper: *"It was assumed that the deviations from spherical symmetry in the blastula could be ignored because it makes no particular difference what form of asymmetry there is. It is, however, important that there are some deviations, for of them, tend to grow. If this happens a new and stable equilibrium is usually reached, with the symmetry entirely gone. The variety of such new equilibria will normally not be so great as the variety of irregularities giving rise to them"*. Turing presented simplified examples of reaction-diffusion systems in which a small deviation from a equilibrium accentuates the differences and others where spatial oscillations appear. Turing also showed different possible kinds of solutions: stationary flat, flat but oscillating in time, stationary but with finite wavelengths and oscillating with a finite wavelength (traveling waves).

Turing presented some characteristics or conditions that a chemical reaction process should have in order to be plausible the equation systems that he presented as example.

Another feature of the pattern formation is their universality in the following sense: different systems that present the same type of instability, when the control parameter is near the bifurcation, also show the same kind of pattern [Mer15].

Reaction-diffusion equations

In a mathematical framework, pattern formation is studied by modelling the physical system with a set of partial differential equations which is called the dynamical system.

The quantity u of some characteristic that can be measured in space (charge, mass, concentration, temperature, biomass, etc..) could be modeled as a density function that specifies a value $u(\mathbf{r}) \in \mathbb{R}$ for each point $\mathbf{r} \equiv (x, y, z)$. The density function u defines the state of the system. If a dynamical model is desired, then the state function u will depend on time, so the explicit function $u(\mathbf{r}, t)$ will specify the evolution of the state.

If there is a dynamical behaviour, then we can specify a vector field called the flux $\mathbf{J}(\mathbf{r}, t)$, which is a vector whose direction points to the velocity of the substance characterised by u , and its magnitude is equal to the infinitesimal quantity of the substance that passes through a plane orthogonal to the velocity direction per unit of time. When the total amount of the quantity is conserved, i.e., when $\int_{\mathbf{r}} u(\mathbf{r}, t_0) d\mathbf{r} = \int_{\mathbf{r}} u(\mathbf{r}, t) d\mathbf{r}$ for any t , then at each point \mathbf{r} the change of the density $u(\mathbf{r}, t)$ should be equal to the negative of the divergence of the flux $\mathbf{J}(\mathbf{r}, t)$:

$$\frac{\partial u}{\partial t} = -\nabla \cdot \mathbf{J}. \quad (2.1)$$

Diffusion occurs when the movement of the quantity u has a tendency to spread out, i. e., a tendency to not have relative maximum or minimum levels, so the movements of the substance will go from the regions that have high levels to the regions that have low ones. Specifically, when the movement of u is only driven by diffusion, then the flux \mathbf{J} in each point goes into the opposite direction of the gradient of u at that point, with a magnitude specified by a coefficient of diffusion D , i.e., $\mathbf{J} = -D\nabla u$, which is known as *Fick's law*. Then, to describe the evolution of u due to diffusion, eq. (2.1) takes the form:

$$\frac{\partial u}{\partial t} = D\nabla^2 u, \quad (2.2)$$

which naturally is called the **diffusion equation**.

Let us consider now two variables to be measured in space that interact among them, let's say u and v . Each one of them diffuses at different rates: D_u and D_v . These variables, for instance, could be chemical concentrations of two substances or biomass of prey and predator species. Now we are no longer held by the conservation restriction, but will allow creation or annihilation of each of the variables, due to its own level and the level of the other variable. So, for each variable, we will add to eq. (2.2) an additional term as a function of u and v . In a chemical context $f_u(u, v)$ and $f_v(u, v)$ are called the reaction terms because they indicate the addition or disappearance of each substance due to the reactions of both or due to an auto-catalytic process. Then, for two variables,

the **reaction-diffusion equation** system has the form:

$$\frac{\partial u}{\partial t} = f_u(u, v) + D_u \nabla^2 u, \quad (2.3a)$$

$$\frac{\partial v}{\partial t} = f_v(u, v) + D_v \nabla^2 v. \quad (2.3b)$$

The reaction terms $f_u(u, v)$ and $f_v(u, v)$ are in general non-linear functions of u and v . Except for very simplified cases, it is not possible to find an analytical solution of (2.3), but a numerical integration is required to trace the evolution from a chosen initial state $u_0(\mathbf{r})$ and $v_0(\mathbf{r})$. In general, a reaction-diffusion equation system may consist of N variables and also crossed diffusion terms, which means that a current of some substances is also affected by the gradient of another one, see eq. (2.27). Although some times we are going to refer about the general case of N variables, most of the systems and examples in this thesis work will use $N = 2$.

Stationary and oscillatory instabilities

It is important to define what is considered as an instability within this framework, and we will use two examples that help us to identify stationary instabilities from oscillatory instabilities.

Steady state or **stationary solutions** of a reaction-diffusion equation system as (2.3) are states $u_s(\mathbf{r})$ and $v_s(\mathbf{r})$ such that $\frac{\partial}{\partial t} u_s = \frac{\partial}{\partial t} v_s = 0$, which means that if they are used as initial condition, then the system at the start is in some sort of equilibrium that generates no change in their subsequent evolution. In principle, there could be several (even infinite) of these steady state solutions, but the simplest task to do is to look for flat solutions. i.e., functions $u_s(\mathbf{r}) = \tilde{u}$ and $v_s(\mathbf{r}) = \tilde{v}$ with a constant value along the space.

In order to search for this flat solutions it is convenient to restrict the problem in a way that only allows flat evolution, i.e., in which only flat states are permitted: $u(\mathbf{r}, t) = u(t)$ and $v(\mathbf{r}, t) = v(t)$. So, the system (2.3) turns into a system of ODE. For a general case with N variables, it will have the form:

$$\frac{d}{dt} \mathbf{u} = \mathbf{f}(\mathbf{u}, \lambda), \quad (2.4)$$

where $\mathbf{u} = (u_1, \dots, u_N)$ is the vector of real variables that represent the state and λ a parameter and $\mathbf{f} = [f_1(\mathbf{u}, \lambda), \dots, f_N(\mathbf{u}, \lambda)]$ is a vectorial function of the variables. The set of equations represented by (2.4) is the **dynamical system** and the space generated by the variables u_1, \dots, u_N is the **phase space**, thus, each point in phase space represent a particular state \mathbf{u} . The evolution $\mathbf{u}(t)$ from some initial condition $\mathbf{u}(0) = \mathbf{u}_0$ is a curve in phase space that indicates a particular trajectory starting at the point \mathbf{u}_0 . The vectorial function \mathbf{f} represent a vector field in the phase space, i.e., it assigns a vector for each point of the phase space which, in particular, is tangent to the trajectory that passes at that point. Here, a steady state solution is a point $\tilde{\mathbf{u}}$ in the phase space such that $\mathbf{f}(\tilde{\mathbf{u}}, \lambda) = \mathbf{0}$, so there are not a tangent vector because the whole trajectory only consist in a single point $\tilde{\mathbf{u}}$; steady

state solutions are also called **equilibrium points**.

Right side of eq. (2.4) can be expanded by Taylor's series around a fixed point $\tilde{\mathbf{u}}$. So in a vicinity of $\tilde{\mathbf{u}}$ the eq. system (2.4) at first order approximation is a linear system with the form:

$$\frac{d}{dt}(\mathbf{u} - \tilde{\mathbf{u}}) = \nabla \mathbf{f}(\mathbf{u} - \tilde{\mathbf{u}}), \quad (2.5)$$

where $\nabla \mathbf{f}$ is the Jacobian matrix such that $\nabla \mathbf{f}_{i,j} = \left. \frac{\partial f_i}{\partial u_j} \right|_{\mathbf{u}=\tilde{\mathbf{u}}}$. This linear system has solutions of the form $\mathbf{u} - \tilde{\mathbf{u}} \propto e^{\sigma_i t} + c.c.$, i.e. the solutions are vectors that point to some direction but with exponential behaviour in time.¹ The complex conjugate is to ensure real values in the solutions, considering that we are dealing with measurable quantities. The values of σ_i ($i = 1..N$), that satisfy the linear equations system correspond to the N eigenvalues of \mathbf{J} , which are, in general, complex. If there is a σ_i such that $Re(\sigma_i) > 0$, then the steady-state $\tilde{\mathbf{u}}$ is **unstable** or we also say that there is an **instability** at the equilibrium point $\tilde{\mathbf{u}}$, because a state $u(t) = \tilde{\mathbf{u}} + \delta \mathbf{u}(t)$ made of a small perturbation from $\tilde{\mathbf{u}}$, within the linear regime only will depend on the evolution of the perturbation which will grow exponentially within the linear regime. If all the eigenvalues fulfill $Re(\sigma_i) < 0$ then the steady-state is **stable** and if the eigenvalue with the highest real part is equal to zero, then the steady-state is called to be **marginally stable**. The eigenvalues σ_i are functions of the parameter λ . A **bifurcation point** is a critical value λ_c of the parameter λ where the fixed point $\tilde{\mathbf{u}}$ loses or gain stability. When $\lambda = \lambda_c$ the system is marginally stable. Let's assume by convention that if $\lambda < \lambda_c$ then the system is the stable and with $\lambda > \lambda_c$ unstable.

For systems extended in space, i.e., systems whose states are also function of the space ($\mathbf{u} = \mathbf{u}(\mathbf{r}, t; \lambda)$) when there is a perturbation around an unstable flat stationary solution, commonly the system evolves going away from the instability and approaching to another steady state but stable solution, or to a time-periodic solution; those instabilities are called **stationary instability** and **oscillatory instability**, respectively. In the following we will present very simple and typical examples of these two kind of instabilities to provide a better intuition of what are they about.

Stationary instabilities

Let us consider the next ODE with $N = 1$:

$$\frac{du}{dt} = \lambda u - u^3. \quad (2.6)$$

If $\lambda > 0$ it has three real stationary solutions: $\tilde{u}_0 = 0$, for any λ and $\tilde{u}_{\pm} = \pm\sqrt{\lambda}$; if $\lambda < 0$ there exists only $\tilde{u}_0 = 0$ as stationary solution. Let's check the stability properties of each solution. The jacobian is only a 1×1 matrix with element $f'(u_i)$ being also the only eigenvalue. We have $f'(0) = \lambda$, so $\tilde{u}_0 = 0$ is stable when $\lambda < 0$, and unstable when $\lambda > 0$, being $\lambda = 0$ the point of bifurcation. And $f'(\pm\sqrt{\lambda}) = -2\lambda$, as the pair of stationary solutions $\tilde{u}_{\pm} = \pm\sqrt{\lambda}$ exist only with $\lambda > 0$, then they are always stable points. In the fig. 2.2 it is shown a bifurcation diagram, in which are plotted

¹Taking into account that the exponential behaviour is only valid mwhile $|\mathbf{u} - \tilde{\mathbf{u}}|$ is small enough to fulfill the first order approximation.

the stationary solutions as function of λ : continuous line represent stable stationary solutions and dashed lines represent unstable solutions.

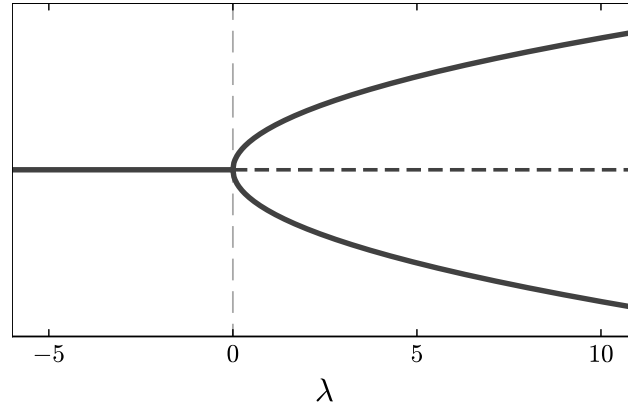


Figure 2.2: Stationary solutions of u with respect to the parameter control λ . Solid/dashed lines stands for stable/unstable solutions. The bifurcation is located at $\lambda = 0$.

The linearization around fixed points only describes an exponential behaviour that occurs in a vicinity of the points, but doesn't show a further trajectory for instabilities points where the state $\mathbf{u}(t)$ goes away from instability. In 1D systems, when the trajectory goes away from an instability, whether it goes infinitely far or whether it falls into a stable fixed point that finds its way. So, as the one in the example (2.6), there are instabilities called **stationary instabilities** in which a small fluctuation from them carries the state into another stationary but stable solution, thus the state in time asymptotically gets steady.

For systems extended in space, small fluctuations around a stationary instability (a flat and unstable stationary solution) are sufficient to take the state into a some steady state, which could have many different shapes, including spatial oscillatory behaviour.

Oscillatory instabilities

The existence of an oscillatory instability in a ODE system requires $N > 1$. A common example that illustrates this behaviour is the following system of non-linear ODE with $N = 2$:

$$\frac{d}{dt}u_1 = \lambda u_1 - \omega u_2 - (u_1^2 + u_2^2)u_1, \quad (2.7a)$$

$$\frac{d}{dt}u_2 = \omega u_1 + \lambda u_2 - (u_1^2 + u_2^2)u_2, \quad (2.7b)$$

with a change of variables where $u_1 = \rho \cos \varphi$ and $u_2 = \rho \sin \varphi$ the system gets a simpler and

decoupled form:

$$\frac{d}{dt}\rho = \lambda\rho - \rho^3, \quad (2.8a)$$

$$\frac{d}{dt}\varphi = \omega. \quad (2.8b)$$

Equation (2.8b) implies that the variable φ advances at a constant rate ω with respect to time. As the equations are decoupled, eq. (2.8a) can be analyzed as eq. (2.6) since has exactly the same form: with $\lambda < 0$ the only fixed point is a stable stationary state with $\rho = 0$, but with $\lambda > 0$ the fix point $\rho = 0$ becomes unstable and appear two more stable points at $\rho = \sqrt{\lambda}$ and $\rho = -\sqrt{\lambda}$ (but in this particular case ρ cannot be negative as a polar variable). Then, with $\lambda > 0$, and due to the dynamics of ρ and the constant angular velocity ω , it can be noticed that near the stationary value $\rho = \sqrt{\lambda}$ there are trajectories that converge to the circle $u_1 = \sqrt{\lambda}\cos(\omega t + \phi_0)$ and $u_2 = \sqrt{\lambda}\sin(\omega t + \phi_0)$ that is called the **limit cycle**. An oscillatory instability is an unstable fixed point such that small fluctuations from it gets a trajectory that converges to a limit cycle. The bifurcation at $\lambda = 0$ that turns on the oscillatory instability it is often called **Hopf bifurcation**.

Patterns classification

Nonequilibrium spatial patterns can be classified by the kind of linear instability that presents some uniform stationary solution. The instabilities appear when some control parameter R of the system exceeds a particular threshold. The instabilities can be divided according to the values of their characteristic wave vector \mathbf{k}_0 or the characteristic frequency ω_0 that reveals at the instability threshold. Patterns with wave vectors or frequencies centered around this characteristic values will grow in the linear regime [CH93].

Non-uniform stationary instabilities present periodic behaviour in space and stationary in time.

There is a lot a patterns with this spatial periodic structure. In 1D, if λ is at the threshold, the pattern will be a single wave with wavelength equal to $2\pi/k_0$, where $k_0 = |\mathbf{k}_0|$. In two or three dimensions other regular patterns, as rolls, squares, labyrinths, hexagons, cubes, etc., can be achieved by a superposition of stationary waves with wavevector in different directions and different amplitude through the space.

Uniform oscillatory instabilities are the ones that induce flat solutions in space but with an oscillatory motion in time.

Non-uniform oscillatory instabilities are instabilities in which the evolution present oscillatory behaviour in time and also in space, so traveling waves appear. In two dimensions can give rise to spiral waves.

Experimental realization of pattern formation

Chemical reactions

The oscillatory behaviour of chemical systems was an outstanding phenomena, not well received at the 1930's by the chemical community when Bray and Liebhafsky published the first experimental results. During the 1950's, Belousov found cyclic behaviour of the color of a mixture

of bromate and cerium ions with citric acid in sulfuric acid; later work of Zhabotinsky on those recipes and characterization of the chemistry led to the recognition among the community until the late 1960's. Zhabotinsky was the first one to use malonic acid to substitute citric acid. In the late 1970's the Bray-Liebhaftsky and Belousov-Zhabotinsky (BZ), both accidentally discovered, and its variants were the only known oscillator reactions that could be replicated in experiments. Theoretical framework developed previously as Lotka-Volterra model, Brusselator model or Oregonator model gave rise during the 1980's to the systematic design of chemical oscillators, based on autocatalytic reactions. In 1990, Kepper and Boissonade presented the chlorite-iodide autocatalytic reaction, that exhibits most of the dynamical behavior of BZ reaction: periodic oscillation, bistability, chemical waves and pattern formation; but simpler than BZ to explain its mechanism and had nice agreement with numerical simulations. Same year, Castets, Dulos Boissonade and Kepper reported the first experimental observation of the emergence of Turing pattern in a non-equilibrium system, using the chlorite-iodide reaction but adding malonic acid. In Epstein and Showalter [ES96] it is shown an overview of experimental works of the chemical oscillators and other nonlinear dynamics as patterns and chaos.

Kepper, Perraud, [DKPBE94] found in the chlorite-iodide-malonic acid (CIMA) reaction a quasi-2D behavior where there is coexistence between Hopf and Turing modes. They reported a dynamics driven mostly by plane waves but with the exception of isolated Turing spots in the core of spirals, see Fig. 3.1. Although Turing spot could be difficult to be seen in the tip of spiral, they show it by making time-averaged image. References [DKPBE94] and [JPM⁺94] claim that the 2D Turing-Hopf spiral is the extended case of the 1D spirals or flip-flop.

2.2 Pattern formation analysis

This section is focused on the linear stability analysis of uniform states in spatial extended systems, where by spatial extended systems we mean that the state \mathbf{u} depends also on some space coordinates \mathbf{r} . With this linear analysis we will show the mechanisms of the emergence of oscillations with particular characteristic frequency in time or space from an instability and also the role that diffusion plays.

Instabilities generated by diffusion

Let's consider a reaction system of two species ($N = 2$), u and v , with no diffusion, i.e., $D_u = D_v = 0$ in (2.3), in a one-dimensional extended space and, for the sake of simplicity, a flat stationary solution in $\tilde{u}(x) = 0$, $\tilde{v}(x) = 0$. Since (2.3) is a system extended in space, the linear analysis is made taking into account a small variation around a flat solution: $u(x, t) = \tilde{u} + \delta u(x, t)$ and $v(x, t) = \tilde{v} + \delta v(x, t)$, where $\delta u(x, t)$ and $\delta v(x, t)$ are functions (perturbations) whose values are infinitesimally small.

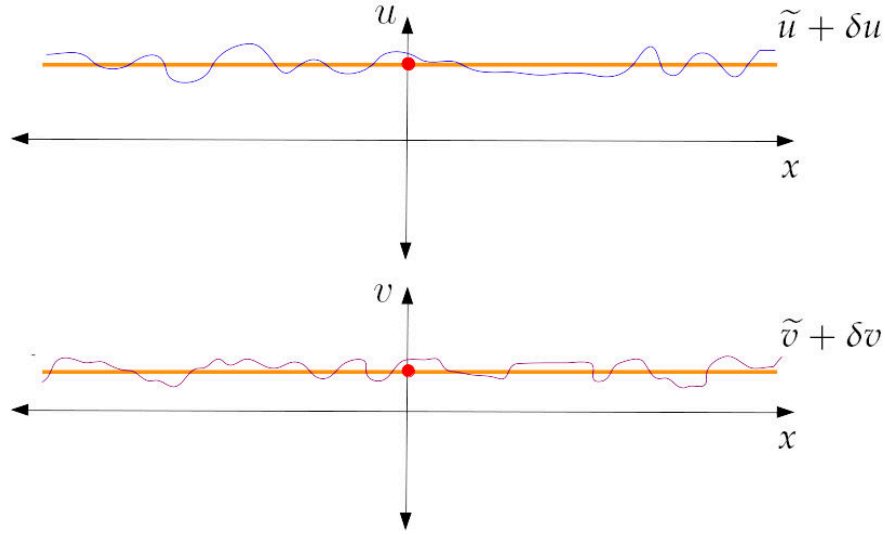


Figure 2.3: Schematic example of small variation around a flat stationary solution as initial condition: $u(x, 0) = \tilde{u} + \delta u(x, 0)$ and $v(x, 0) = \tilde{v} + \delta v(x, 0)$. Flat yellow lines stand for \tilde{u} and \tilde{v} , respectively.

These perturbations (if they are smooth), as any smooth function, can be represented as Fourier integrals, $\delta u(x, t) = \int \alpha_\lambda(t) e^{i\lambda x} d\lambda$ and $\delta v(x, t) = \int \beta_\lambda(t) e^{i\lambda x} d\lambda$. Within the linear regime it is enough to calculate separately one of the modes and the evolution of the perturbations $\delta u(x, t)$ and $\delta v(x, t)$ will be the integral of the evolution of all the λ -modes.

For example, only analysing the evolution of the k -mode, the perturbations will have the simple form:

$$\delta_k u(x, t) = \alpha_k(t) e^{ikx} + c.c., \quad (2.9a)$$

$$\delta_k v(x, t) = \beta_k(t) e^{ikx} + c.c., \quad (2.9b)$$

where $\alpha_k(t)$ and $\beta_k(t)$ are complex values that determine the amplitude and phase of the mode, and *c.c.* indicates the complex conjugate to restrict perturbations to real quantities.

We had assumed that the perturbations $\delta_k u$ and $\delta_k v$ are around the zero solution $\tilde{u} = 0$, $\tilde{v} = 0$, thus, now it is only needed to substitute (2.9) in the original system (2.3), with $D_u = D_v = 0$, to obtain the linear system around the flat stationary solution. A linear ODE system of the Fourier coefficients will arise:

$$\begin{bmatrix} d\alpha_k/dt \\ d\beta_k/dt \end{bmatrix} = \begin{bmatrix} a_{11} & a_{12} \\ a_{21} & a_{22} \end{bmatrix} \begin{bmatrix} \alpha_k(t) \\ \beta_k(t) \end{bmatrix}, \quad (2.10)$$

where $a_{ij} = \nabla \mathbf{f}_{i,j}$ are the coefficients of the jacobian matrix A , and $\mathbf{f} = [f_u(u, v), f_v(u, v)]$ are the reaction functions. The solution to this system has an exponential form:

$$\begin{bmatrix} \alpha_k(t) \\ \beta_k(t) \end{bmatrix} = \begin{bmatrix} c^1 \\ c^2 \end{bmatrix} e^{\sigma t}, \quad (2.11)$$

where $\sigma = \sigma(k; \lambda)$ is a complex value that can be function of k and also of the parameters of the system $\lambda = (\lambda_1, \lambda_2, \dots)$. The vector $(c^1, c^2)^T$ is complex but with constant elements and the only dependence on time is on the exponential behaviour. Placing (2.11) in (2.10), a eigenvalue problem is obtained:

$$\sigma \begin{bmatrix} c^1 \\ c^2 \end{bmatrix} = A \begin{bmatrix} c^1 \\ c^2 \end{bmatrix}, \quad (2.12)$$

which implies that σ is an eigenvalue of A and $(c^1, c^2)^T$ its corresponding eigenvector.

In this case, the coefficients of A do not depend on k therefore, neither does σ , which means that the amplitudes $\alpha_k(t)$ and $\beta_k(t)$ of any mode k will grow or decay at the same rate, indicated by the greatest real part of the eigenvalues. The eigenvalues are $\sigma_{\pm} = \frac{1}{2}trA \pm \frac{1}{2}\sqrt{(trA)^2 - 4detA}$, which implies that the trace of A determines the stability, and the case where $detA$ is negative we have eigenvalues of different sign.

Let us assume that $[\tilde{u}(x) = 0, \tilde{v}(x) = 0]$ is a stable point, implying that the real part of both eigenvalues of A , σ_1 and σ_2 are negative thus:

- i) $trA < 0$,
- ii) $detA > 0$.

The case where both a_{11} and a_{22} are negative is of no interest on this text, and the case with both positive does not fulfill the condition i) $trA < 0$. Thus, a_{11} and a_{22} have opposite sign, let's assign $a_{11} > 0$ and $a_{22} < 0$ to work with. It means that the reaction functions at first order have a positive feedback for the u species, and negative for v . Then, conditions i) and ii) imply $|a_{11}| < |a_{22}|$ and also that a_{12} and a_{21} have opposite sign.

Now we are going to add diffusion for both species, with diffusion coefficients D_u and D_v , recalling eq. (2.3), and with the same reaction functions as in the jacobian matrix A (2.10).

Substituting (2.9) in (2.3):

$$\begin{bmatrix} d\alpha_k/dt \\ d\beta_k/dt \end{bmatrix} = \begin{bmatrix} a_{11} - D_u k^2 & a_{12} \\ a_{21} & a_{22} - D_v k^2 \end{bmatrix} \begin{bmatrix} \alpha_k \\ \beta_k \end{bmatrix}. \quad (2.13)$$

And now $A' = A + k^2 \begin{bmatrix} -D_u & 0 \\ 0 & -D_v \end{bmatrix}$ the new coefficient matrix for the system (2.16).

The condition that we need to switch the stability property with the inclusion of diffusion is for the real part of one of the eigenvalues to become positive, and it is obtained when $detA' < 0$, which gives eigenvalues of opposite sign.

$$detA' = a_{11}a_{22} - k^2(D_u a_{11} + D_v a_{22}) + k^4 D_u D_v - a_{12}a_{21}.$$

The only term that could contribute negatively to $detA'$ is $-k^2(D_u a_{11} + D_v a_{22})$. If the diffusion coefficients are of equal magnitude, then that term reduces to $-k^2 D_u (trA)$ which is positive, since

$\text{tr}A < 0$. So, D_u has to be sufficiently bigger than D_v not only to make $D_u a_{11} + D_v a_{22}$ a positive quantity, but also to ensure that $k^2(D_u a_{11} + D_v a_{22}) > \det A + k^4 D_u D_v$ to fulfill the condition $\det A' > 0$.

In summary, if the diffusion of the species that has positive feedback is sufficiently larger than the diffusion of the other species, then the original stability without diffusion can be broken.

Dispersion relations and growth rate curves.

The coefficient $\sigma = \sigma(k; \lambda)$ of the exponential function (2.11) that determine the evolution of the amplitudes of the Fourier modes, characterized by different k and a set of parameters λ , plays a protagonist role in pattern formation theory. Only in the linear approximation - in a vicinity of the flat stationary solution (\tilde{u}, \tilde{v}) - a solution dependent on time from any initial small perturbation can be seen as a superposition of Fourier's modes

$$\begin{bmatrix} u(x, t) \\ v(x, t) \end{bmatrix} = \begin{bmatrix} \tilde{u} \\ \tilde{v} \end{bmatrix} + \int_k \begin{bmatrix} \alpha(t; k, \lambda) \\ \beta(t; k, \lambda) \end{bmatrix} e^{ikx} dk + c.c.,$$

where the Fourier amplitudes have only an exponential dependence on time:

$$\begin{bmatrix} \alpha(t; k, \lambda) \\ \beta(t; k, \lambda) \end{bmatrix} = \begin{bmatrix} c^1(k; \lambda) \\ c^2(k; \lambda) \end{bmatrix} e^{\sigma(k, \lambda) t}.$$

As each Fourier amplitude grows or decays at different rates, the whole shape of the solutions will change over time. In this example we assumed that we have a single control parameter λ . The exponential function can be factorized as $e^{\sigma_R t} e^{i\sigma_I t}$, where $\sigma_R \equiv \text{Re}(\sigma)$ and $\sigma_I \equiv \text{Im}(\sigma)$. The imaginary part of σ gives temporal oscillations with frequency $\omega_c = \sigma_I$, which is called the **Hopf mode**. The real part of σ is what determines the growth rate. The explicit function $\sigma_R(k)$ of the growth rate with respect to the mode k is called **dispersion relation**, and the plot σ_R against k is known as *growth-rate curve*.

By varying the control parameter λ , the whole growth-rate curve changes. The stability bifurcation occurs when the control parameter takes a value λ_c such that there is at least one point that touches the k -axis at k_c with the rest of the curve is below it, thus, when $\lambda = \lambda_c$ only the mode k_c is marginally stable and the rest of the modes will decay with time; that is, λ_c is the parameter such that there exists a k_c which fulfills: $\sigma_R(k_c; \lambda_c) = 0$, $\sigma'_R(k_c; \lambda_c) = 0$ (where $\sigma'_R(k; \lambda)$ is the derivative of σ_R with respect to k) and $d^2\sigma_R/dk^2|_{k=k_c} < 0$, i.e, $\sigma_R(k; \lambda_c)$ has relative maximum in k_c with a level of zero.

So, from an initial condition containing the k_c mode in a Fourier decomposition, the evolution of the system will hold only the k_c mode and, if $\omega_c \neq 0$, it will also hold the Hopf mode:

$$\begin{bmatrix} u(x, 0) \\ v(x, 0) \end{bmatrix} \xrightarrow{t \rightarrow \infty} \begin{bmatrix} c^1_{k_c}(\lambda) \\ c^2_{k_c}(\lambda) \end{bmatrix} e^{i\omega_c t} e^{ik_c x} + c.c.. \quad (2.14)$$

If λ is not equal to λ_c but slightly greater, then the mode k_c and some of the modes in a small interval around k_c will have an exponential growth in the linear regime, the growth of the mode k_c will be bigger than any other. For example, if $k_c = 0$ and $\omega_c \neq 0$ then a uniform but oscillatory behaviour in time will prevail. Then the instability in 1D is defined by k_c and ω_c which are called characteristic wave number and characteristic frequency, respectively. In a space of more than one dimension there is a characteristic wave vector \mathbf{k}_c . In fact, particularly in isotropic systems, there can be several wave vectors coexisting in a pattern. This can give rise to crystalline patterns as discussed, for instance, by W. Klein and coauthors [KL06].

This is the main mechanism of pattern formation. From an arbitrary initial condition $(u(x), v(x))$ that is near a flat stationary but unstable solution indicated by a control parameter that is placed very near the bifurcation point, the modes with wave number $k \in [k_c - \varepsilon_1, k_c + \varepsilon_2]$ and frequency ω_c in time, will grow while the rest of the modes will decay; where $[k_c - \varepsilon_1, k_c + \varepsilon_2]$ is the interval in which $\sigma_R(k)$ is positive. That means that, under some conditions, from a random initial configuration of a system made out of small fluctuations from an instability, even when each random initial configuration is very different, in all cases the further evolution will generate a similar global structure that is carved in a general form by k_c and ω_c .

The shape of the growth-curves shows the types of instabilities that a determined system could present, see Fig. 2.4.

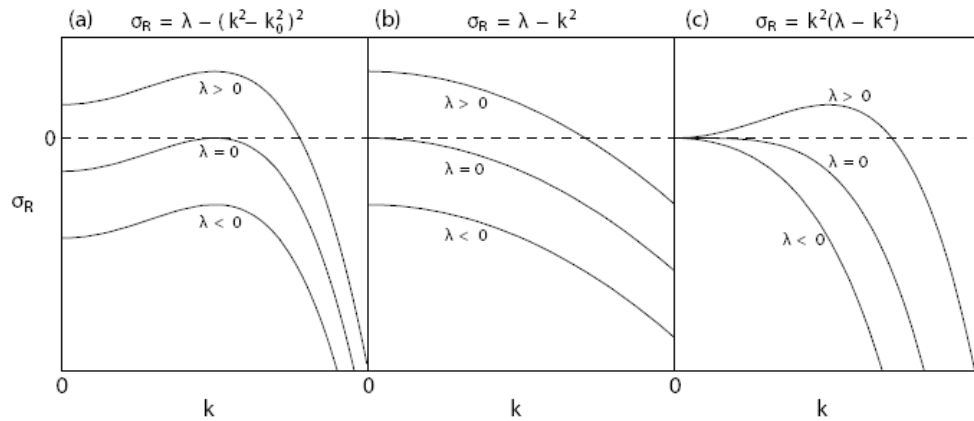


Figure 2.4: Different types of growth-rate curves, taking $\lambda_c = 0$. Figure from [Mer15].

From the explicit expression of the surviving mode in the linear regime, previously expressed in (2.14) we can easily identify four types of instability, due to their linear exponential response which is determined by the particular shape of the growth-rate curve:

- **Uniform stationary instability** ($\omega_c = 0, k_c = 0$). This instability push the evolution into different but stable flat solutions. When there are, for example, two different stable solutions as in Fig. 2.2, we say that bistability exists and the asymptotic solution in a extended 1D space could be a combination of both, divided by a transition region that is called a **front** or domain wall.

-**Non-uniform stationary instability** ($\omega_c = 0, k_c \neq 0$). This is the case when a Turing mode arises in the bifurcation instability. It evolves into stationary patterns with spatial oscillations.

-**Uniform non-stationary instability** ($\omega_c \neq 0, k_c = 0$). The case when a Hopf mode is the principal in the bifurcation, it evolves as a flat but oscillatory state.

-**Non-uniform non-stationary instability** ($\omega_c \neq 0, k_c \neq 0$). It corresponds to a mixed state which evolves into traveling waves. It occurs when the maximum wavenumber k is greater than zero but also $\omega_c \neq 0$.

Non-uniform stationary instability

In the rest of the section we are going to use the FitzHugh-Nagumo (FHN) model only as an example of a reaction-diffusion equation to show the basic mechanisms of pattern formation from certain type of instabilities. It is a model that was developed by Richard FitzHugh (published in 1961) when he was trying to simplify the Hodgkin and Huxley's equations for the flow through the squid giant axon membrane of sodium and potassium ions. At relatively the same time, Jin-Ichi Nagumo built a circuit whose behaviour was similar to the simplified equations.

The FHN model has two types of substances or fields in space: $u(\mathbf{r})$ and $v(\mathbf{r})$, where u generates a positive feedback (activator) for both substances, while v provides a slower negative feedback; and the reaction function of the activator u has a nonlinear component which depends negatively in u . Along the time, FitzHugh-Nagumo model has been widely used by mathematicians, physicists, biologists and engineers, and is one of the prototypical example to understand instabilities and pattern formation [IF06].

The specific version of the FHN model that we are going to use is:

$$\partial_t u = u - u^3 - v + \nabla^2 u, \quad (2.15a)$$

$$\partial_t v = \epsilon(u - av) + \delta \nabla^2 v. \quad (2.15b)$$

Looking at the lineal behaviour around the flat stationary solution $u(x) = 0$ and $v(x) = 0$, the substance u acts as an activator that contributes positively to the growth of u and v , while v acts as an inhibitor. All the coefficients (a, ϵ, δ) are positive real values and $a < 1$.

As the last examples, the linearization is obtained by using a Fourier mode k (2.9) as a perturbation function from the zero solution $u(x) = 0$ and $v(x) = 0$. The resultant linear ODE system is

$$\begin{bmatrix} d\alpha_k/dt \\ d\beta_k/dt \end{bmatrix} = \begin{bmatrix} 1 - k^2 & -1 \\ \epsilon & -\epsilon a - \delta k^2 \end{bmatrix} \begin{bmatrix} \alpha_k \\ \beta_k \end{bmatrix}. \quad (2.16)$$

As in any linear system of ODEs, we will look for exponential solutions with growth rate σ_R . The dispersion relations of the system are:

$$\sigma_{\pm}(k; \epsilon, a, \delta) = \frac{1}{2}(1 - k^2 - \epsilon a - \delta k) \pm \frac{1}{2}\sqrt{(1 - k^2 + \epsilon a + \delta k)^2 - 4\epsilon}. \quad (2.17)$$

In this example let us consider the case $\epsilon > 1/a$.

For low values of k the expression inside the square root is negative (taking into account that $a < 1$), so the real part of σ is $\frac{1}{2}(1 - k^2 - \epsilon a - \delta k)$, when $k = 0$ we have $\sigma_R(0) = 1/2 - \epsilon a/2 < 0$ due to the premise on ϵ . As k increases from zero, $\sigma_R(k)$ decreases, until the expression inside the square root becomes positive so $Re[\sigma_+(k)] = \sigma_+(k)$.

We are going to take δ as our control parameter. The next step is to find for which δ (in terms of the other parameters a and ϵ), the growth curve touches the k -axis in just one point k_c , and to specify that point k_c also in terms of the rest of the parameters. To find δ_c and k_c we have two non-linear equations that must hold: $\sigma_+(k_c; \delta_c) = 0$ and $\sigma'_+(k_c; \delta_c) = 0$, where σ' stands for the derivative of sigma with respect to k ; and also we have to ensure that the second derivative evaluated in k_c is negative.

With some algebra the non-linear system reduces to this pair of equations:

$$0 = (1 - k_c^2)(\epsilon a + \delta_c k_c) - \epsilon, \quad (2.18a)$$

$$0 = \delta_c(1 - k_c^2) - 2k_c(\epsilon a + \delta_c k_c). \quad (2.18b)$$

With the command *Solve* of the software *Wolfram Mathematica 11.0* four analytical solutions of the system (2.18) were obtained. Among the four solutions we took only the one in which k_c and δ_c were real and positive. The explicit expression in terms of the parameters a and ϵ are:

$$k_c = \sqrt{\Psi(a)}, \quad (2.19a)$$

$$\delta_c = \frac{1}{2}a\epsilon[9/a - 5 + 3\Psi(a)]\sqrt{\Psi(a)}, \quad (2.19b)$$

where $\Psi(a) = 1 - \frac{3}{2a} + \frac{\sqrt{9-8a}}{2a}$.

To get the complete expression similar to (2.14) of the first mode k_c to grow beyond the bifurcation point δ_c , it is necessary to solve the eigenvector problem of the linear matrix with components evaluated in k_c and δ_c :

$$\begin{aligned} \begin{bmatrix} 0 \\ 0 \end{bmatrix} &= \begin{bmatrix} 1 - k_c^2 - \sigma_+(k_c; \delta_c) & -1 \\ \epsilon & -\epsilon a - \delta_c k_c^2 - \sigma_+(k_c; \delta_c) \end{bmatrix} \begin{bmatrix} c_{k_c}^1 \\ c_{k_c}^2 \end{bmatrix}, \\ &= \begin{bmatrix} 1 - \Psi(a) - 0 & -1 \\ \epsilon & \frac{1}{2}a\epsilon[9/a - 3 + 3\Psi(a)]\Psi(a) - 0 \end{bmatrix} \begin{bmatrix} c_{k_c}^1 \\ c_{k_c}^2 \end{bmatrix}. \end{aligned}$$

Once we have the corresponding eigenvector

$$\begin{bmatrix} c_{k_c}^1 \\ c_{k_c}^2 \end{bmatrix} \propto \begin{bmatrix} 1 \\ 1 - \Psi(a) \end{bmatrix},$$

we get the complete expression of the first mode k_c that emerges from the instability at the bifurcation point δ_c :

$$\left[\frac{1}{1 - \Psi(a)} \right] e^{ik_c x} + c.c.. \quad (2.20)$$

The instability bifurcations that lead to a non-uniform stationary state are called **Turing bifurcation** and the spatial oscillations for each wave number are called **Turing modes**. In our example, the Turing bifurcation is found at δ_c .

Uniform oscillatory instability

We are going to use the same FitzHugh-Nagumo model, but this time with no diffusion for the substance v , i.e., with $\delta = 0$:

$$\partial_t u = u - u^3 - v + \nabla^2 u, \quad (2.21a)$$

$$\partial_t v = \epsilon(u - av). \quad (2.21b)$$

Again, the coefficients (a, ϵ) are positive real values and $a < 1$.

In this case ($\delta = 0$), the dispersion relation is:

$$\sigma_{\pm}(k; \epsilon, a) = \frac{1}{2}(1 - k^2 - \epsilon a) \pm \frac{1}{2}\sqrt{(1 - k^2 + \epsilon a)^2 - 4\epsilon}. \quad (2.22)$$

Now we are going to take ϵ as the control parameter.

There are two possibilities, the square root term is real or imaginary at the bifurcation point ϵ_c .

Lets assume that the square root is a real value. If this is the case, then, there are two ways in which we can make σ reach a value of zero: either both terms of $\sigma(k; \epsilon, a)$ are zero or they cancel each other. Let's check if it is possible for the magnitude of both terms to be equal. Comparing the squares of each term, with $\epsilon \neq 0$ we have:

$$\begin{aligned} (1 - k^2 + \epsilon a)^2 - 4\epsilon &< \\ (1 - k^2 + \epsilon a)^2 - 4\epsilon a &= (1 - k^2)^2 - 2k^2\epsilon a - 2\epsilon a + \epsilon^2 a^2 \\ &< (1 - k^2)^2 + 2k^2\epsilon a - 2\epsilon a + \epsilon^2 a^2 = (1 - k^2 - \epsilon a)^2, \end{aligned}$$

Since $(1 - k^2 + \epsilon a)^2 - 4\epsilon < (1 - k^2 - \epsilon a)^2$ for any case where $\epsilon \neq 0$, then we can not get $Re[\sigma_{\pm}(k_c; \epsilon_c, a)] = 0$ if the square root term is real, which means that at the bifurcation point σ is complex.

The real part of σ is $\sigma_R(k; \epsilon, a) = \frac{1}{2}(1 - k^2 - \epsilon a)$ and its derivative with respect to k , $\sigma'_R(k; \epsilon, a) = -k$ (and the double derivative is negative). Then the maximum value of the growth-rate curve is located at $k = 0$, and the value of ϵ that modifies the curve to get $\sigma_R(0; \epsilon_c, a) = 0$ is $\epsilon_c = 1/a$.

The characteristic frequency is $\omega_c = \frac{1}{2}\sqrt{4\epsilon_c - (1 - k_c^2 + \epsilon_c a)^2} = \sqrt{1-a}/\sqrt{a}$. Since the characteristic wave number is $k_c = 0$, the first mode growing in the instability consists of a uniform solution for u and v that oscillates in time, which is called the **Hopf mode**:

$$\begin{bmatrix} 1 \\ 1 - i\frac{\sqrt{1-a}}{\sqrt{a}} \end{bmatrix} e^{i\omega_c t} + c.c.. \quad (2.23)$$

The imaginary value in the second element of the eigenvector indicates the shift in the phase of the oscillations of v with respect to u .

Codimension-2 Hopf-Turing instability

Let's revisit the FitzHugh-Nagumo model (2.15) with the positive parameters (a, ϵ, δ) , and $a < 1$. We can adjust both ϵ and δ in order to make the growth-rate curve touch the k -axis in two points without exceeding $\sigma_R = 0$, having simultaneously two marginal stable points: one with $k = 0$ and $\omega_c \neq 0$, the other with $k_c \neq 0$ and $\omega = 0$. With this particular selection of parameters ϵ_c and δ_c , the stationary solution $u(x) = 0$ and $v(x) = 0$ becomes a **Hopf-Turing instability**. Codimension- n refers to the number n of parameters that are needed to adjust to get a particular bifurcation point.

Then, the codimension-2 point Hopf-Turing instability of the system (2.15) is reached with

$$\epsilon_c = 1/a, \quad (2.24)$$

$$\delta_c = \frac{1}{2}[9/a - 5 + 3\Psi(a)]\sqrt{\Psi(a)}, \quad (2.25)$$

where $\Psi(a) = 1 - \frac{3}{2a} + \frac{\sqrt{9-8a}}{2a}$. The characteristic frequency for the Hopf mode is $\omega_c = \sqrt{1-a}/\sqrt{a}$ and the characteristic wavenumber of the Turing mode is $k_c = \sqrt{\Psi(a)}$.

Since almost all the Fourier components of the perturbation will decay within a first order approximation, the evolution of the state around the zero solution will be mainly driven by the Hopf and Turing modes:

$$\begin{bmatrix} u(x, t) \\ v(x, t) \end{bmatrix} \approx \begin{bmatrix} 1 \\ 1 - i\frac{\sqrt{1-a}}{\sqrt{a}} \end{bmatrix} H(x, t)e^{i\omega_c t} + \begin{bmatrix} 1 \\ 1 - \Psi(a) \end{bmatrix} T(x, t)e^{ik_c x} + c.c., \quad (2.26)$$

where $H(x, t)$ and $T(x, t)$ are the amplitudes of the *Hopf* mode and the *Turing* mode, respectively, which are defined in time and space.

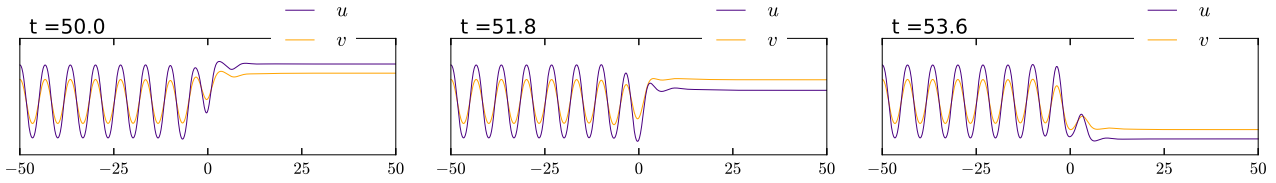


Figure 2.5: A 1D example of a system with its parameters located near codimension-2 point Hopf-Turing instability. Purple/yellow colors stands for u (activator)/ v (inhibitor), respectively; when x is sufficiently larger than zero only Hopf mode holds, and when x is sufficiently lower than zero only Turing mode takes place. Around $x = 0$ is a mixed mode, which consists in the Hopf-Turing front that divide both regions.

Weak non-linear analysis: Amplitude equations

The analysis of last section was restricted to the linear behaviour of a reaction-diffusion systems (2.27), from infinitesimal fluctuations around a flat stationary solution, and only gives a description of the mode corresponding to the characteristic wave number k_c or the characteristic frequency ω_c of the system. One step further is to deal with a tiny or weak effect of non-linearity of the system.

When the control parameter λ is slightly above λ_c , not only the mode k_c grows exponentially as well as some continuous range of k around it, this range being that in which the growth-rate curve is above zero. The approximation of this behaviour does not involve integrating the different survival modes in this narrow range of k , and instead we consider that as all the modes within the unstable range are very similar to k_c , the interference will be considerable only at long distances with respect to the space wavelength or long times with respect the period of time oscillations -depending on the type of instability-, so the effect of this slow interference will be expressed only as changes of the complex amplitude A of the characteristic mode. The amplitude will then be a function of space and time, $A = A(x, t)$, and the **weak non-linear analysis** is the deduction of a differential equation from which $A(x, t)$ can be obtained. If it is a codimension- n instability, then the analysis will bring a system of n coupled complex amplitude equations. The deduction of the amplitude equations is based on a perturbation method, using expansion series around a stationary flat solution and around the bifurcation point of the control parameter λ . Since the amplitudes change slowly in time and space with respect to the oscillation modes, slow variables scaled by powers of λ are used in this analysis to separate the behaviour of the amplitude and the exponential factor of the mode. At the end, some equations generated from the expansion will give conditions that have to fulfill the amplitude of the first term of the expansion, which corresponds to the associated critical mode. In the following it is shown how this analysis method works.

Consider a general reaction-diffusion type system:

$$\frac{\partial}{\partial t}|u\rangle = f(|u\rangle) + \mathbf{D}\nabla^2|u\rangle, \quad (2.27)$$

where $|u\rangle \equiv (u_1, \dots, u_N)^T$ are density functions of chemical substances (with N being an inte-

ger), $f(|u\rangle)$ are functions containing linear and nonlinear terms of the functions u_i that correspond to chemical reactions or interactions, and \mathbf{D} is a matrix associated with diffusion and cross-diffusion [VE09].

If the state is in a vicinity of a non-uniform stationary instability, then it can be approximated as:

$$|u(\mathbf{r}, t)\rangle \approx |\tilde{u}\rangle + |e_T\rangle A(\mathbf{r}, t)e^{ik_c x} + c.c., \quad (2.28)$$

or if it is in a vicinity of a uniform oscillatory instability:

$$|u(\mathbf{r}, t)\rangle \approx |\tilde{u}\rangle + |e_H\rangle A(\mathbf{r}, t)e^{i\omega_c t} + c.c., \quad (2.29)$$

where $|\tilde{u}\rangle$ is a stationary and spatially uniform state, and $|e_i\rangle$ is the corresponding eigenvector evaluated at the bifurcation point (with $i \in \{H, T\}$).

The derivation of a system of two equations for the real and imaginary part of the amplitude $A(\mathbf{r}, t)$ is called **weak nonlinear analysis**, because it is valid only when we consider the following two points:

1. The amplitudes are small enough so that the state is near the instability point.
2. The control parameter is near the bifurcation point.

The idea of this approach is to consider that the variations in the space domain and time of the amplitude $A(\mathbf{r}, t)$ are small or “weak”. So, it could be natural to think about different scales, the scale of the oscillation period of the growing mode and the scales in each direction and time in which the variation of the amplitude is considerable. For the sake of this method, it is useful to define slow space and time variables so the amplitude only will be a function of them, while the oscillation term in (2.28) or (2.29) remains as a function of the space (or time) variable of the original scale. To exemplify the idea, let us consider a 1D space domain and also assume that $|\tilde{u}\rangle = |0\rangle$ is a uniform oscillatory instability (in this case, $|0\rangle$ stands for null vector). So

$$|u\rangle \approx |e_H\rangle \tilde{A}(X, T)e^{i\omega_c t} + c.c., \quad (2.30)$$

and only depends on the regular variable t and the slow variables $X = \lambda^p x$ and $T = \lambda^q t$, where p and q are the exponents of λ that define the scale of each one of the slow variables. The explicit function \tilde{A} of the slow variables comes from the original amplitude function $A(x, t)$ from eq. (2.29): $\tilde{A}(X, T) = A(\lambda^{-p}X, \lambda^{-q}T)$. As there is no harmonic term oscillation in space, the amplitude is the only factor that varies along the x -axis but at a slow pace, so only a slow space variable X and not regular variable x appears in the state $|u\rangle$. Due to the use of different scales in the domain variables, this method is also called **multiple-scale analysis**.

Let λ be the control parameter, and let us set $\lambda_c = 0$ as the point of the Hopf bifurcation. An approximation of the state $|u\rangle$ near the bifurcation point $\lambda = 0$ can be made with an expansion of $|u\rangle$ in powers of λ^s , that goes beyond than (2.30) with higher order terms:

$$|u\rangle = \lambda^s |u_0\rangle + \lambda^{2s} |u_1\rangle + \lambda^{3s} |u_2\rangle + \dots \quad (2.31)$$

After expansion, the expression (2.31) is needed to be substituted into the original equation system (2.27) at some order. But the expansion terms $|u_j\rangle$, in principle, explicitly depend on normal and slow variables, which has to be taken into account in the derivative operators by carefully applying the chain rule; it will be equivalent to make the following substitution:

$$\frac{\partial}{\partial t} \rightarrow \frac{\partial}{\partial t} + \lambda^q \frac{\partial}{\partial T}, \quad (2.32)$$

$$\frac{\partial}{\partial x} \rightarrow \lambda^p \frac{\partial}{\partial X}, \quad (2.33)$$

then non linear equations of the variables in $|u_j\rangle$ will be obtained for each corresponding order $j = 0, 1, 2, \dots$ of the form

$$\mathcal{M}|u_j\rangle = |R_j\rangle, \quad (2.34)$$

where \mathcal{M} is a linear operator and $|R_j\rangle$ is vector column that depends on lower order ($j - 1$) contributions of the solution.

What follows is to obtain the explicit form of the different $|R_j\rangle$. For $j = 0$ we have the equation $\mathcal{M}|u_0\rangle = |0\rangle$, that corresponds with the linearization of the system around the instability. The growing mode has the characteristic frequency ω_c , so:

$$|u_0\rangle = |e_H\rangle B(X, T) e^{i\omega_c t} + c.c., \quad (2.35)$$

First, with explicit solution $|u_0\rangle$ we get $|R_1\rangle$, and solving the respective differential equation we will get $|u_1\rangle$ which is needed for explicit expression of $|R_2\rangle$, and so on.

For each $|R_j\rangle$ that we get, we have to ensure that equation (2.34) has solution; it will be needed that the terms R_j fulfill its respective solvability condition, which will be explained in the following subsection. At the end, the solvability conditions will provide the amplitude equations that we are looking for.

Solvability conditions

We got equations of the form $\mathcal{M}|u_j\rangle = |R_j\rangle$ for each order j , and we are interested in states whose dependence in regular (not slow) variables is periodic and bounded, so they can be expressed in terms of trigonometric polynomials. But the linear operator \mathcal{M} has no inverse, thus it is not clear that these equations have solution, the two possibilities are: the solutions do not exist or they have infinite solutions.

In our example (2.35) the only regular variable is t ; thus some arbitrary vector $|w\rangle$ with the characteristics desired can be seen as a trigonometric polynomial series: $|w\rangle = \sum_n \begin{bmatrix} a_n \\ b_n \end{bmatrix} e^{ni\omega_c t} + c.c.$, where a_n and b_n are complex functions of the slow variables (X, T) .

When the operator \mathcal{M} acts on $|w\rangle$ it give rise to another vector $|z\rangle$ which also can be viewed as a trigonometric polynomial series:

$$\mathcal{M}|w\rangle = |z\rangle = \begin{bmatrix} c_0 \\ d_0 \end{bmatrix} + \begin{bmatrix} c_1 \\ d_1 \end{bmatrix} e^{i\omega_c t} + \begin{bmatrix} c_2 \\ d_2 \end{bmatrix} e^{2i\omega_c t} + \begin{bmatrix} c_3 \\ d_3 \end{bmatrix} e^{3i\omega_c t} + \dots + c.c.. \quad (2.36)$$

As $|w\rangle$ is an arbitrary vector, the right side of (2.36) is the general form of the image of \mathcal{M} . For each term in $|w\rangle$, the operator \mathcal{M} does not change the order of $e^{ni\omega_c t}$ but only transforms the vector coefficients corresponding to each order.

A common feature of the linear operators \mathcal{M} that comes from reaction-diffusion equations of two variables (u, v) is that their null space is not trivial but has dimension one and is proportional to the first order trigonometric term $e^{i\omega_c t}$, which has a particular implication on the image. Then the image (2.36) has a restriction: the vector $\begin{bmatrix} c_1 \\ d_1 \end{bmatrix}$ can not be any arbitrary vector in \mathbb{C}^2 but only a vector that belongs to a certain subspace of dimension one; let us suppose that the vector $|g\rangle \in \mathbb{C}^2$ generate the subspace that defines this part of the image, i.e., $\begin{bmatrix} c_1 \\ d_1 \end{bmatrix} = \kappa |g\rangle$, where κ is some complex coefficient.

It is convenient to use an orthogonal basis of \mathbb{C}^2 related to the image: $\{|g\rangle, |h\rangle\}$, given some inner product $\langle \cdot | \cdot \rangle$, where $|g\rangle$ generates the coefficient vector $(c_1, d_1)^T$ of the image of \mathcal{M} and $|h\rangle$ is orthogonal to $|g\rangle$, i.e., $\langle h | g \rangle = 0$. Now we have a way to check if eq. (2.34) has infinite solutions or not a single one. The key is to look for the terms of $|R_j\rangle$:

$$|R_j\rangle = \begin{bmatrix} q_{j0} \\ s_{j0} \end{bmatrix} + \begin{bmatrix} q_{j1} \\ s_{j1} \end{bmatrix} e^{i\omega_c t} + \begin{bmatrix} q_{j2} \\ s_{j2} \end{bmatrix} e^{2i\omega_c t} + \begin{bmatrix} q_{j3} \\ s_{j3} \end{bmatrix} e^{3i\omega_c t} + \dots + c.c.,$$

and focus on the coefficients of the first order term; the term $\begin{bmatrix} q_{j1} \\ s_{j1} \end{bmatrix} e^{i\omega_c t}$ must be in the image of \mathcal{M} ,

thus it is required for $|r_{j1}\rangle \equiv \begin{bmatrix} q_{j1} \\ s_{j1} \end{bmatrix}$ to be proportional to $|g\rangle$ or orthogonal to $|h\rangle$. As q_{j1} and s_{j1} are functions of the amplitudes $B(X, T)$ and its complex conjugate, some conditions can be imposed on $B(X, T)$ to ensure $|r_{j1}\rangle$ to be orthogonal to $|h\rangle$.

The orthogonality is prescribed by the equation:

$$\langle h | r_{j1} \rangle = 0. \quad (2.37)$$

The equations (2.37) for $i = 0, 1, \dots$ are the so called **solvability conditions**, and from those conditions, a partial differential equation for the complex amplitude $B(X, T)$ can emerge, with the form $\frac{\partial B}{\partial T} = \tilde{\mathcal{F}}(B, \bar{B})$, where $\tilde{\mathcal{F}}(B, \bar{B})$ is some nonlinear function of B, \bar{B} its complex conjugate and its spatial derivatives.

Let us recall that B is only the amplitude of $|u_0\rangle$ but we are looking for the state $|u\rangle$ which will be approximated up to the first term of expansion (2.31) and also we want to express it in terms of

regular variables:

$$|u\rangle \approx \lambda^s |u_0\rangle = |e_H\rangle A(x, t) e^{i\omega_c t} + c.c., \quad (2.38)$$

so $B(\lambda^p x, \lambda^q t) = \lambda^{-s} A(x, t)$ and substituting it in the partial equation for B and changing the differential operators by the chain rule to rescale (X, T) so that we can work now only with the regular variables x and t , obtaining finally the complex **amplitude equation** with the form:

$$\frac{\partial A}{\partial t} = \mathcal{F}(A, \bar{A}), \quad (2.39)$$

where $\mathcal{F}(A, \bar{A}) = \lambda^q \tilde{\mathcal{F}}(\lambda^{-s} A, \lambda^{-s} \bar{A})$.

When two modes simultaneously grow from an unstable state, two complex amplitude equations are needed (or four equations of real functions). For example if we are in a Hopf and Turing bifurcation, the amplitude equations system will have the form:

$$\frac{\partial H}{\partial t} = \mathcal{F}_H(H, \bar{H}, T, \bar{T}), \quad (2.40a)$$

$$\frac{\partial T}{\partial t} = \mathcal{F}_T(H, \bar{H}, T, \bar{T}), \quad (2.40b)$$

where $H(x, t)$ is the complex amplitude of Hopf mode and $T(x, t)$ the complex amplitude for the Turing mode; \bar{H} and \bar{T} are the complex conjugates of H and T .

In the appendix we show the deduction of the amplitude equations from a complex Ginzburg-Landau system in 2D, which takes the Hopf and two perpendicular Turing modes (3.1) thus, we obtained three complex amplitude equations (3.2).

Amplitude equations for uniform oscillations

The FitzHugh-Nagumo model, with $\delta = 0$ and $a < 1$ (2.21) has a uniform oscillating instability ($k_c = 0, \omega_c \neq 0$), as we have seen previously, that is reached when $\epsilon = \epsilon_c$ (having found previously that $\epsilon_c = 1/a$), and becomes unstable when $\epsilon < \epsilon_c$. In this example the extended space will consist of a 2D domain. Our goal is to obtain the amplitude equation, which will be a partial differential equation having $\mathcal{A}(x, y, t)$ as the unknown multivariate function. When $\epsilon \lesssim \epsilon_c$ an approximation of the state near the zero solutions has the form of (2.29):

$$\begin{bmatrix} u \\ v \end{bmatrix} \approx \begin{bmatrix} c^1 \\ c^2 \end{bmatrix} \mathcal{A}(x, y, t) e^{i\omega_c t} + c.c.. \quad (2.41)$$

It is useful to change the control parameter by $\mu = (\epsilon_c - \epsilon)/\epsilon_c$ because μ measures the deviation from the Hopf bifurcation point in a dimensionless scale; the bifurcation is located at $\mu = 0$ and with $\mu > 0$ the system becomes unstable. As we are in a 2D space, instead of a characteristic wave number, we have a wave vector $\mathbf{k} = k_x \mathbf{i} + k_y \mathbf{j}$. The growth-rate curve is given by $\sigma(\mu) = (\mu - k^2)/2$, where $k^2 = k_x^2 + k_y^2$. When $\mu > 0$, the range of k that contains the unstable

modes is the one in which $\sigma(k) \geq 0$, and that occurs when $k \in [0, \sqrt{2\mu}]$. The maximum growth rate is $\mu/2$ located at $k = 0$. As the region of unstable modes grows proportionally to $\sqrt{\mu}$, then the slow spatial variables will be scaled by $\sqrt{\mu}$, i.e., $X = \sqrt{\mu}x$ and $Y = \sqrt{\mu}y$. The maximal growth rate corresponds to the mode $k_c = 0$ and its magnitude scales linearly with μ , as this mode does not contribute with oscillations in space, but only in time at frequency ω_c , the slow variable in time will scale also in a linear form: $T = \mu t$.

Expansion (2.31) (with μ instead of λ) will be placed in both sides of the FHN system (2.15), so it will be derived by the operators $\partial/\partial t$ and ∇^2 . The amplitudes of the approximation will depend exclusively on the slow variables (X, Y, T) and only the exponential factors will have dependence on the regular variables. Since there is no $e^{ik_c x}$ nor $e^{ik_c y}$, the right side of (2.31) won't depend on the regular spatial variables, but only on (X, Y, t, T) . Thus, when we place expansion (2.31) into (2.15), we have to take into account the chain rule to replace the derivative operators:

$$\begin{aligned} \frac{\partial}{\partial t} &\rightarrow \frac{\partial}{\partial t} + \mu \frac{\partial}{\partial T}, \\ \frac{\partial}{\partial x} &\rightarrow \sqrt{\mu} \frac{\partial}{\partial X}, \quad \frac{\partial}{\partial y} \rightarrow \sqrt{\mu} \frac{\partial}{\partial Y}. \end{aligned} \quad (2.42)$$

The smallest order for μ in the expansion (2.31) is μ^s . When the expansion is substituted in the cubic term u^3 of eq. (2.21a), the term of minimum order that comes out from it is proportional to μ^{3s} , and the term of minimum order that comes out from $\nabla^2 u = \mu \nabla_{[X,Y]}^2 u$ is proportional to μ^{s+1} (where $\nabla_{[X,Y]}^2 \equiv \partial_X^2 + \partial_Y^2$). We need the two terms to be of the same order, thus $s = 1/2$. Then, the expansion (2.31) around $u(x, y) = 0$, $v(x, y) = 0$ and around $\mu = 0$ takes the form:

$$\begin{bmatrix} u \\ v \end{bmatrix} \approx \sqrt{\mu} \begin{bmatrix} u_0 \\ v_0 \end{bmatrix} + \mu \begin{bmatrix} u_1 \\ v_1 \end{bmatrix} + \mu^{3/2} \begin{bmatrix} u_2 \\ v_2 \end{bmatrix}. \quad (2.43)$$

The form of the first term is proposed as the characteristic mode with frequency ω_c and its amplitude $B(X, Y, T)$ depending only in slow variables:

$$\begin{bmatrix} u_0 \\ v_0 \end{bmatrix} = \begin{bmatrix} c^1 \\ c^2 \end{bmatrix} B(X, Y, T) e^{i\omega_c t} + c.c., \quad (2.44)$$

the term $(u_1, v_1)^T$ will be deduced to get $|R_2\rangle$ and it won't be necessary to deduce $(u_2, v_2)^T$ since with $|R_2\rangle$ we'll be able to get the solvability condition that gives rise to the amplitude equation.

Substituting the expansion (2.43) into (2.21) and taking into account the slow variables in the derivative operators, we get rid of terms of an order greater than 3/2 and three equations are obtained, corresponding to each different order of μ .

For $\sqrt{\mu}$ order:

$$\frac{\partial u_0}{\partial t} = u_0 - v_0, \quad (2.45a)$$

$$\frac{\partial v_0}{\partial t} = \epsilon_c (u_0 - av_0). \quad (2.45b)$$

For μ order:

$$\frac{\partial u_1}{\partial t} = u_1 - v_1, \quad (2.46a)$$

$$\frac{\partial v_1}{\partial t} = \epsilon_c(u_1 - av_1). \quad (2.46b)$$

For $\mu^{3/2}$ order:

$$\frac{\partial u_2}{\partial t} + \frac{\partial u_0}{\partial T} = u_2 - v_2 - u_0^3 + \frac{\partial^2 u_0}{\partial X^2} + \frac{\partial^2 v_0}{\partial X^2}, \quad (2.47a)$$

$$\frac{\partial v_2}{\partial t} + \frac{\partial v_0}{\partial T} = \epsilon_c(u_2 - av_2) - \epsilon_c(u_0 - av_0). \quad (2.47b)$$

The linear operator corresponding to this example is:

$$\mathcal{M} = \begin{bmatrix} \frac{\partial}{\partial t} - 1 & 1 \\ -\epsilon_c & \frac{\partial}{\partial t} + 1 \end{bmatrix}. \quad (2.48)$$

The solution of $\mathcal{M} \begin{bmatrix} u_0 \\ v_0 \end{bmatrix} = \begin{bmatrix} 0 \\ 0 \end{bmatrix}$ fixes the direction of the eigenvector proposed in (2.44), whose components can be selected as $e = 1, f = 1 - i\omega_c$. The equations (2.45) and (2.46) are identical, thus they share the same family of solutions. Using this solution as the explicit form of $(u_0, v_0)^T$ and $(u_1, v_1)^T$ that can be substituted in (2.47), and gives the explicit form of $\mathcal{M} \begin{bmatrix} u_2 \\ v_2 \end{bmatrix} = |R_2\rangle$:

$$\mathcal{M} \begin{bmatrix} u_2 \\ v_2 \end{bmatrix} = \begin{bmatrix} -\frac{\partial B}{\partial T} - 3|B|^2 B + \frac{\partial^2 B}{\partial X^2} + \frac{\partial^2 B}{\partial Y^2} \\ -(1 - i\omega_c)\frac{\partial B}{\partial T} - \epsilon_c B + (1 - i\omega_c)B \end{bmatrix} e^{i\omega_c t} + \begin{bmatrix} -B^3 \\ 0 \end{bmatrix} e^{3i\omega_0 t} + c.c.. \quad (2.49)$$

But there is an important issue to take into account: from subsection 2.2 in the linear analysis, we knew that the null space of \mathcal{M} is not trivial but it has dimension one. Recalling eq. (2.23), is straightforward that the kernel of \mathcal{M} can be spanned by the vector $|e_1\rangle e^{i\omega_c t}$,

where $|e_1\rangle = \begin{bmatrix} 1 \\ 1 - i\omega_c \end{bmatrix}$, with $\omega_c = \sqrt{1-a}/\sqrt{a}$.

Let us take as inner product in \mathbb{C}^2 the canonical hermitian inner product. First we want to find the image that corresponds only to terms proportional to $e^{i\omega_c t}$, as the image is of dimension one, it is only needed a vector $|e_2\rangle$ that does not belong to the null space, to get $\mathcal{M}|e_2\rangle e^{i\omega_c t}$ which generates the image of the order desired. If we select some vector $|e_2\rangle$ orthogonal to $|e_1\rangle$ we ensure that does not belong to the null space.

Selecting $|e_2\rangle = \begin{bmatrix} -1 - i\omega_c \\ 1 \end{bmatrix}$ we have $\langle e_2 | e_1 \rangle = 0$.

As $|e_2\rangle$ do not belong to the null space, the image that is proportional to $e^{i\omega_c t}$ will be for sure

generated by the vector

$$\begin{aligned} \mathcal{M}|e_2\rangle e^{i\omega_c t} &= \begin{bmatrix} \frac{\partial}{\partial t} - 1 & 1 \\ -\epsilon_c & \frac{\partial}{\partial t} + 1 \end{bmatrix} \begin{bmatrix} -(1 + i\omega_c)e^{i\omega_c t} \\ e^{i\omega_c t} \end{bmatrix} \\ &= b \begin{bmatrix} 1 \\ (1 + i\omega_c) \end{bmatrix} e^{i\omega_c t}, \quad \text{with } b = (1 + a)/a. \end{aligned} \quad (2.50)$$

As we can see in (2.50), this term of the image is generated by $|g\rangle e^{i\omega_c t}$ where $|g\rangle = \begin{bmatrix} 1 \\ 1 + i\omega_c \end{bmatrix}$. Now we can get a vector $|h\rangle$ orthogonal to $|g\rangle$:

$$|h\rangle = \begin{bmatrix} -1 + i\omega_c \\ 1 \end{bmatrix}. \quad (2.51)$$

In eq. (2.49) we can see the trigonometric polynomial expansion of $|R_2\rangle$, where the vector coefficient $|r_{21}\rangle$ of first order trigonometric term $e^{i\omega_c t}$ is

$$|r_{21}\rangle \equiv \begin{bmatrix} -\frac{\partial B}{\partial T} - 3|B|^2 B + \frac{\partial^2 B}{\partial X^2} + \frac{\partial^2 B}{\partial Y^2} \\ -(1 - i\omega_c)\frac{\partial B}{\partial T} - \epsilon_c B + (1 - i\omega_c)B \end{bmatrix} \quad (2.52)$$

To restrict $|r_{21}\rangle e^{i\omega_c t}$ to be in the image of \mathcal{M} , the solvability condition $\langle h|r_{21}\rangle = 0$ is imposed and gives the equality

$$0 = 2\frac{\partial B}{\partial T} + 3(1 + i\omega_c)|B|^2 B - (1 + i\omega_c)\left(\frac{\partial^2 B}{\partial X^2} + \frac{\partial^2 B}{\partial Y^2}\right) - \omega_c(\omega_c + i)B. \quad (2.53)$$

Now, if we combine (2.44) with the expression (2.43) approximated only at first order we have that

$$\begin{bmatrix} u \\ v \end{bmatrix} \approx \sqrt{\mu} \begin{bmatrix} 1 \\ 1 - i\omega_c \end{bmatrix} B(X, Y, T) e^{i\omega_c t} + c.c.,$$

and comparing this expression with the original form of the Hopf mode presented in (2.41), we see that $\mathcal{A}(x, y, t) = \sqrt{\mu} B(\sqrt{\mu}x, \sqrt{\mu}y, \mu t)$. From the solvability condition (2.53) we obtained an equation for the complex amplitude \mathcal{A} :

$$\frac{\partial \mathcal{A}}{\partial t} = \frac{1}{2}\mu\omega_c(\omega_c + i)\mathcal{A} - \frac{3}{2}(1 + i\omega_c)|\mathcal{A}|^2\mathcal{A} + \frac{1}{2}(1 + i\omega_c)\nabla^2\mathcal{A}, \quad (2.54)$$

which is the desired amplitude equation.

Equation (2.54) has the following general form that can be adjusted by three parameters (α, β, μ) and is known as the **Complex Ginzburg-Landau equation**:

$$\frac{\partial \mathcal{A}}{\partial t} = \mu\mathcal{A} - (1 + i\beta)|\mathcal{A}|^2\mathcal{A} + (1 + i\alpha)\nabla^2\mathcal{A}. \quad (2.55)$$

This equation describes the behaviour of the amplitude of the characteristic mode ω_c near the bifurcation of any Hopf instability.

Frequency locking

Nonlinear systems with a Hopf instability have, naturally, a self-sustained oscillator near the instability bifurcation. If an external periodic force is applied it could, under certain conditions, synchronise its frequency, changing its original frequency ω_0 into another different but similar frequency driven by the forcing. This phenomenon is a nonlinear resonance mechanism known as **frequency locking**. The synchronization occurs when the amplitude γ of the forcing is strong enough and when a rational scalar of the forcing frequency ω_f is near the original frequency ω_0 , i. e., when $(m/n)\omega_f \approx \omega_0$, with integers m and n . When the locking occurs, the system deviates from its original frequency ω_0 and instead takes a frequency equal to $(m/n)\omega_f$ determined by the external forcing, and is called the $n : m$ resonance [PR07, Knu99]. The difference between the original frequency and the synchronised one is called the detuning: $\nu = \omega_0 - (m/n)\omega_f$. As $|\nu|$ is set bigger, a stronger forcing is needed to lock the oscillations of the system; the region in the $\nu - \gamma$ parameter space where the frequency locking takes place is called the **Arnold resonance tongue**.

Let us assume that system (2.27) goes through a primary oscillatory Hopf instability and is also externally forced at a certain frequency [LHMS04]. Near the onset and depending on the forcing amplitude and frequency, the medium will exhibit either unlocked or locked oscillations which will obey the **forced complex Ginzburg-Landau (FCGL)** equation [Gam85, EIT87, CE92, EHM99]:

$$\frac{\partial A}{\partial t} = (\mu + i\nu)A - (1 + i\beta)|A|^2 A + (1 + i\alpha)\nabla^2 A + \gamma\bar{A}^{n-1}, \quad (2.56)$$

where A is a complex amplitude of the primary Hopf mode weakly varying in space and time, \bar{A} complex conjugate, n is an integer associated with the $n : 1$ resonance, μ is the distance from the Hopf onset, ν is the difference between natural and the forcing frequencies, and γ is the forcing amplitude. In this context, frequency locking corresponds to asymptotically stationary solutions to (2.56).

Equation (2.56) can be derived by symmetry considerations [Mer15]. The $n : 1$ resonance takes place when an original system (2.27) has a Hopf instability with characteristic frequency ω_0 and is subjected to periodic forcing with frequency $\omega_f \approx n\omega_0$. In the vicinity of the Hopf bifurcation, the state has the form:

$$|u\rangle \approx |e_H\rangle \mathcal{A} e^{i\omega_0 t} + c.c. = |e_H\rangle A e^{-i\nu t} e^{i\omega_0 t} + c.c. = |e_H\rangle A e^{i(\omega_f/n)t} + c.c.. \quad (2.57)$$

The new variable $A = \mathcal{A} e^{i\nu t}$ is introduced, where $\nu = \omega_0 - \omega_f/n$. The solutions such that A is stationary, correspond to **resonant** or **frequency locked** oscillations, which implies that the oscillations get restrained to the frequency ω_f/n .

The amplitude equation for A can be obtained by substituting $\mathcal{A} = A e^{-i\nu t}$ in CGL equation (2.55) and by adding another term that will be proportional to the forcing amplitude. The periodic forcing breaks the continuous time translation symmetry that the system (2.55) had, but leaves a discrete time translation symmetry: the equation should be invariant under translations that are multiple of the forcing period $\tau_f = 2\pi/\omega_f$. Applying the translation $t \rightarrow t + \tau_f$ to the state (2.57),

the amplitude takes the form $Ae^{i(\omega_f/n)(t+\tau_f)} = Ae^{i(\omega_f/n)t}e^{i(2\pi/n)t}$ thus, the amplitude equation should be invariant under the transformation $A \rightarrow Ae^{i(2\pi/n)t}$. Eq. (2.55) is already unaffected by this transformation, but if we want to add a term proportional to the forcing amplitude, this term has to be of the form \bar{A}^{n-1} in order to be invariant under the transformation. In summary, substitution of $\mathcal{A} = Ae^{-i\nu t}$ in CGL equation (2.55) will give an equation for the amplitude A of resonant oscillations, the time derivative will display the term $i\nu A$ and the addition of the forcing term needs to be a $\gamma\bar{A}^{n-1}$. This way eq. (2.56) is obtained.

Since the Hopf-Turing bifurcation in (2.56) arises only for $n = 2$, the study of Hopf-Turing spatially localized states applies to only in 2:1 frequency locking. In the 2:1 resonance case, Eq. 2.56 admits two uniform non-trivial (π shifted) solutions that exist for [CE92, YHM⁺02, YEHM04b]

$$\gamma > \gamma_b = \frac{|\nu - \mu\beta|}{\sqrt{1 - \beta^2}}. \quad (2.58)$$

This bistability region is commonly called the classical (Arnold) 2:1 resonance tongue even in the context of the spatially extended media, see region I in Figs. 3.1(b,c). Moreover, bistability of uniform π shifted states, can also lead to formation of inhomogeneous solutions [CL90, GCOSM90, YEHM04b, BYK08], such as labyrinthine patterns, spiral waves, and spatially localized (a.k.a. oscillons). However, it has been shown that nonuniform 2:1 resonant patterns may in fact exist also outside the 2:1 resonance [YHM⁺02], $\gamma < \gamma_b$, i.e., in a region where stationary non-trivial uniform solutions are absent. The resonant condition is obtained through stripe (Turing state) nucleation due to the propagation of a Hopf-Turing front, i.e., an interface that bi-asymptotically connects Hopf and Turing states, as shown in Fig. 3.1(a).

1D localized patterns and homoclinic snaking

When there is bistability (coexistence) of two modes in a 1D domain system, front solutions can exist. A single front regularly moves in time towards some direction, until one of the modes invades completely the other. The direction of the moving front is regulated by the control parameter λ . The velocity of the front is zero for some $\lambda = \lambda_m$, which is called Maxwell point. Having a solution with two fronts, these fronts separate the domain making one of the modes to be localized or pinned in a region. For some systems, such that one of the modes is non-uniform, this region is stationary not only in the Maxwell point, but in a range around it, $\lambda_1 < \lambda_m < \lambda_2$.

Having two modes in 1D domain, there is a lot of possible localized pattern solutions, simply by changing the pinning domain or the phase of wavelength. The aim is to find the stable localized pattern solutions.

Let us first take two stationary modes: uniform stationary mode and Turing mode (non-uniform stationary). A way to analyze the possible stable localized solutions, is to solve the time-independent version of eq. 2.27 selecting a parameter near Maxwell point λ_m . There are several numerical methods to solve non-linear ODE. The solution will be a stationary profile $|u_\lambda(x)\rangle$ that fulfils certain conditions selected; it can be stable or unstable. Then we change slightly the parameter λ and see how it changes the previous solution; as we move λ back when reaches a bifurcation, the new

solutions will present hysteresis. Usually for some λ near λ_m there are multiple stationary states. To make a schematic way to present the solutions, their stability and bifurcations it is convenient to obtain a scalar from the solution state $|u_\lambda(x)\rangle$. A particular election could be the L_2 -norm: $\|u_\lambda(x)\|^2 = \langle u_\lambda(x)|u_\lambda(x)\rangle$. Then the bifurcation diagram can be made by plotting $\|u_\lambda\|$ vs λ ; the curve near the Maxwell point commonly has a snaking behaviour, see Fig. 2.6.

In the book [Mer15], Meron uses the modified Swift-Hohenberg equation: $\partial_t u = \lambda u + \alpha u^2 - u^3 - (\nabla^2 + k_c^2)^2 u$ as example. There is a range in the parameter space where uniform stationary solution and stationary periodic pattern coexist. In the example, the pinned or localized mode will be the uniform one, and the periodic pattern around it. In the bifurcation diagram Fig. 2.6 different stable localized solutions are presented in the region $\lambda_1 < \lambda < \lambda_2$.

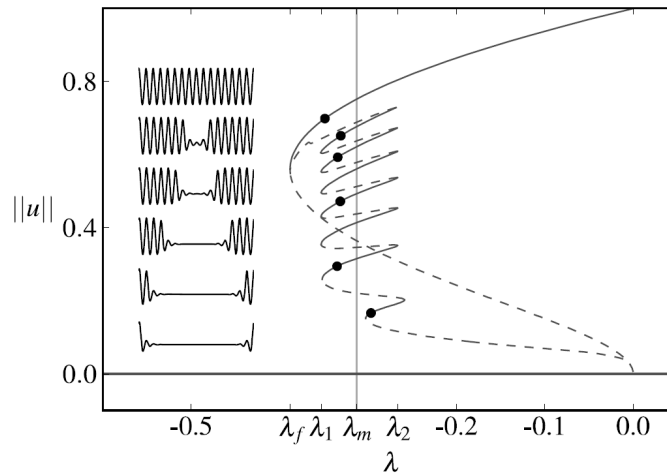


Figure 2.6: Bifurcation diagram of stationary solutions of the modified SH equation. The vertical axis $\|u\|$ represents the L_2 norm of $u(x)$. At the left of the plot are represented $u(x)$ stationary profiles, each with different size of the localized mode, and each represented by a dot in the bifurcation diagram. Solid/dashed lines stand for stable/unstable solutions. The vertical line is at the Maxwell point $\lambda = \lambda_m$. Figure and caption from [Mer15].

“The complete bifurcation diagram of solutions is more involved and contains more periodic-pattern branches and many more hybrid states involving mixtures of uniform and periodic pattern domains of different sizes. Since this localized solutions are homoclinic orbits in some appropriately defined phase space, this behaviour is called **homoclinic snaking**; where a homoclinic orbit in this context is a trajectory in phase space that emanates from a saddle point at $x \rightarrow -\infty$ and returns to it at $x \rightarrow +\infty$ ” [Mer15].

When one of the modes is a Hopf mode, then there are no stationary solutions, but we can still have a stable pinning behaviour. Thus, the procedure to obtain the bifurcation diagram, although is very similar than the one just described above, but it has to take into account also time integration over the Hopf period [TMB⁺13].

2.3 Previous research in the field

Coexistence of periodic stationary and temporal patterns: Hopf-Turing bifurcation

In a vicinity of the codimension-2 Hopf-Turing instability, the solution $|u(x, t)\rangle$ can be approximated by:

$$|u\rangle \approx |\tilde{u}\rangle + |e_H\rangle \tilde{H}(\sqrt{\epsilon}x, \epsilon t) e^{i\omega_c t} + |e_T\rangle \tilde{T}(\sqrt{\epsilon}x, \epsilon t) e^{ik_c x} + c.c.,$$

where $|\tilde{u}\rangle$ is a spatially uniform state that goes through an instability, *c.c.* is complex conjugate, \tilde{H} and \tilde{T} are slowly varying Hopf and Turing amplitudes in space and time, $|e_H\rangle$ and $|e_T\rangle$ are eigenvectors of the critical Hopf frequency (ω_c) and Turing wavenumber (k_c) at a codimension-2 onset, respectively. Multiple-scale analysis using the above ansatz, leads to a generic set of Hopf and Turing (HT) amplitude equations [Kee76, Kid80, JBB⁺01, DW99]:

$$\frac{\partial H}{\partial t} = m_1 H - m_2 |H|^2 H - m_3 |T|^2 H + m_4 \frac{\partial^2 H}{\partial x^2}, \quad (2.59a)$$

$$\frac{\partial T}{\partial t} = n_1 T - n_2 |T|^2 T - n_3 |H|^2 T + n_4 \frac{\partial^2 T}{\partial x^2}, \quad (2.59b)$$

where $m_{1,2,3,4} \in \mathbb{C}$ and $n_{1,2,3,4} \in \mathbb{R}$, with the explicit functions $H(x, t) = \tilde{H}(\sqrt{\epsilon}x, \epsilon t)$ and $T(x, t) = \tilde{T}(\sqrt{\epsilon}x, \epsilon t)$. Notably, system (2.59) is a reduction of (2.27) and reproduces well the flip-flop behavior [DKPBE94, JPM⁺94, Bha07, DWLDB96, DBDW⁺95], i.e., a spatially localized Turing state embedded in π shifted Hopf oscillations.

Frequency locking outside the resonant region

The intriguing and rich dynamics of the Hopf-Turing bifurcation have been demonstrated not only in the CIMA reaction [DKPBE94, DKBE90] but also have been found to be fundamental in broadening the 2:1 frequency locking behavior in the periodically forced Belousov-Zhabotinsky chemical reaction [YHM⁺02]. Consequently, we focus here on the framework of frequency locking in spatially extended oscillatory media to study both the 2D Hopf-Turing localization and its relation to further increase of the 2:1 resonance region, in general.

Particularly in this research project we work on the FCGL equation (2.56) with $n = 2$ (the 2:1 frequency locking), let us present it in terms of the real and imaginary part of the amplitude,

$u = \text{Re}(A)$ and $v = \text{Im}(A)$:

$$\begin{aligned} \frac{\partial u}{\partial t} &= (\mu + \gamma)u - \nu v + \nabla^2 u - \alpha \nabla^2 v \\ &\quad + (-u + \beta v)(u^2 + v^2), \end{aligned} \quad (2.60a)$$

$$\begin{aligned} \frac{\partial v}{\partial t} &= \nu u + (\mu - \gamma)v + \alpha \nabla^2 u + \nabla^2 v \\ &\quad + (-\beta u - v)(u^2 + v^2), \end{aligned} \quad (2.60b)$$

which have the form of a reaction-diffusion equation(2.27) with linear and non-linear terms of the reaction functions of u and v , and also diffusion and cross-diffusion terms. In a linear regime around the zero solution, with a forcing amplitude γ bigger than μ , u acts as an activator and v as an inhibitor.

The codimension-2 Hopf-Turing bifurcation is an instability of the trivial uniform state $A = 0$ at $\lambda = 0$ and $\gamma = \gamma_c$ [YEHM04b], with $\omega_c = \nu\alpha/\rho$, $k_c^2 = \nu\alpha/\rho^2$, $\gamma_c = \nu/\rho$ and $\rho = \sqrt{1 + \alpha^2}$. Notably, the Hopf-Turing bifurcation occurs outside the resonance region as $\gamma_c < \gamma_b$. Multiple time scale analysis resulted with coefficients [YEHM04b] for the Hopf-Turing amplitude equations (2.59):

$$m_1 = \lambda - i\frac{\gamma - \gamma_c}{\alpha}, \quad m_2 = 4 + i2\beta\frac{2\rho^2 + 1}{\alpha\rho}, \quad (2.61a)$$

$$m_3 = 8\rho(\alpha + \rho) + i\left\{4\beta\frac{2\alpha\rho(\alpha + \rho) + 3\rho + \alpha}{\alpha} - 4(\alpha + \rho)\right\}, \quad m_4 = 1 + i\rho, \quad (2.61b)$$

$$n_1 = \lambda + \rho\frac{\gamma - \gamma_c}{\alpha}, \quad n_2 = 6\rho(\alpha + \rho)\left(1 - \frac{\beta}{\alpha}\right), \quad (2.61c)$$

$$n_3 = 4\left(2 - 3\frac{\beta}{\alpha}\right), \quad n_4 = 2\rho^2. \quad (2.61d)$$

Specifically, stability analysis of pure Hopf and Turing modes showed that for $\beta = \beta_c < 5\alpha/9$ these two uniform states coexist and thus it is possible to form a heteroclinic connection between them [YEHM04b], i.e., a front solution. The Hopf-Turing front is stationary (Fig. 2.10(b)) at

$$\gamma_N = \gamma_c + \frac{\mu}{\rho} \left[\sqrt{\frac{3}{4}(2\alpha - 3\beta)(\alpha - \beta)} - \alpha \right], \quad (2.62)$$

and propagates otherwise [OGB98], with $\gamma > \gamma_N$ the Turing state invades the Hopf state (Fig. 2.10(a)) and vice-verse (Fig. 2.10(c)). Moreover, the presence of the stationary front serves as an organizing center for the homoclinic snaking phenomena [TMB⁺13] that would be discussed in the next subsection.

The dominance of the asymptotically stationary Turing mode in region II, $\gamma_N < \gamma < \gamma_b$, extends thus, the classical frequency locking domain (region I) once spatially extended patterns are formed [YHM⁺02, YEHM04a]. Notably, Turing type solutions are in fact standing-waves in the context of the original system (2.27). Figures 3.1(b,c) show the classical resonance region for a single oscillator (region I) and the extended frequency locked region due to the dominance of a spatially extended Turing mode (region II). Our interest is thus, in the unlocked region III

($\gamma_T < \gamma < \gamma_N$ in Figures 3.1(b,c)) where, despite the Hopf mode dominance (i.e., Hopf state is favorable over the Turing state), 2D resonant *localized* comb-like states may still form (see Figure 3.1(a)), with

$$\gamma_T = \gamma_c - \frac{\mu}{4\rho}(\alpha + 3\beta), \quad (2.63)$$

which is the stability onset of the Turing mode [YEHM04b]. For $\gamma < \gamma_T$ only Hopf oscillations persist, i.e., region IV.

In what follows, we use γ as a control parameter while keeping all other parameters constant. Notably, we limit the scope to the coexistence region between the Hopf and Turing modes [YEHM04b], with ($\beta < 5\alpha/9$) and $\gamma_T < \gamma < \min\{\gamma_H, \gamma_b\}$, where $\gamma_H = \gamma_c + \mu(\alpha - 3\beta)/\rho$, see Figure 2.11. As such the localized 2D solutions in region III are resonant states and thus extend further the frequency locking boundary, as portrayed in Figure 3.1.

Flip-flop dynamics, depinning and homoclinic snaking

The behaviour known as “flip-flop” occurs when a small 1D stripe structure made of few wavelengths is surrounded on both sides by Hopf oscillations, each side oscillates with a phase jump of π , see Fig. 2.7. The amplitude of the oscillations reaches zero in the core of the Turing structure [JPM⁺94]. This behaviour has been observed in experiments with chemical reactions [DKPBE94] and also in numerical simulations [PDWD⁺93].

In Fig. 2.8(a) we show the evolution in time of the field $u = \text{Re}(A)$; while in Fig. 2.8(b) we show the profile of the Hopf and Turing amplitudes corresponding to flip-flop.

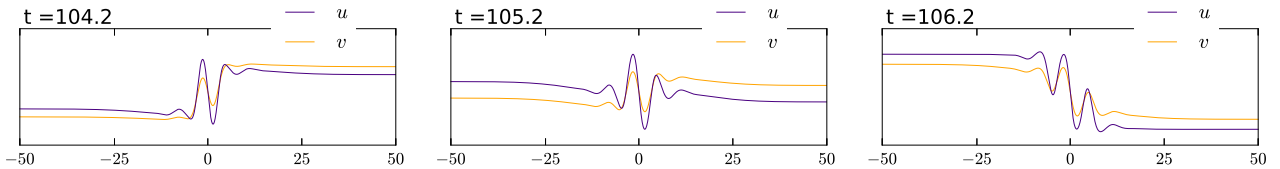


Figure 2.7: 1D space domain x in horizontal axis. Direct numerical integration of (2.60) in 1D, showing the flip-flop and the depinning dynamics; purple/yellow colors stands for u/v , respectively; $\gamma = 2.01$ while other parameters $\mu = 0.5$, $\nu = 2.2$, $\beta = 0$, $\alpha = 0.5$.

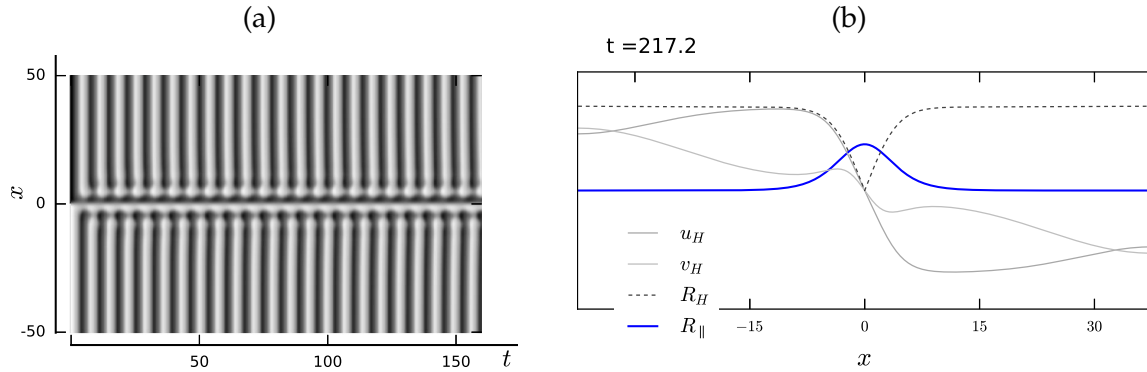


Figure 2.8: Two different pictures are shown, FCGL and HT amplitude equations:

(a) Time in horizontal axis and position x in vertical axis. Direct numerical integration of (2.60) in 1D, showing the flip-flop and the depinning dynamics; light/dark colors indicate max/min value of the $u = \text{Re}(A)$ field, respectively. $\gamma = 2.01$.

(b) Position in horizontal axis and amplitudes in vertical axis. A snapshot (with the time fixed in $t=217.2$) from numerical integration of Hopf-Turing amplitude equations (2.59) corresponding to FCGL, i.e. with parameters m_i and n_i taken from (2.61), $\gamma = 2.02$. Continuous gray lines correspond to Hopf amplitudes $u_H = \text{Re}(H)$, $v_H = \text{Im}(H)$ and dashed line to $R_H = |H|$. Blue line correspond to the absolute value of Turing amplitude mode, $R_{||} = |T_{||}|$. Starting in $t = 0$ with a Hopf-front, the Turing spot (blue line) in the middle of the front emerges and becomes stable while the Hopf amplitude remains constant outside the Turing domain. $\gamma = 2.01$.

* The notation $T_{||}$ is used to emphasize that the Turing mode direction is parallel to the direction of the Hopf front. In 1D has no relevance, but it is important to specify it in a 2D domain.

The other parameters are $\mu = 0.5$, $\nu = 2.2$, $\beta = 0$, $\alpha = 0.5$ for both insets.

Hopf-Turing spatial localization, pinning, and depinning in 1D have been studied in detail with the Brusselator model by Tzou *et al.* (2013), who have shown the relation to the homoclinic snaking phenomenon [TMB⁺13].

The Brusselator model used by Tzou was

$$\begin{aligned}\partial_t u &= D\partial_x^2 u + E - (B+1)u + vu^2, \\ \partial_t v &= \partial_x^2 v + Bu - vu^2.\end{aligned}$$

Specifically, two snaking behaviours were outlined, see Fig. 2.9:

- (i) Standard (vertical) snaking: if the Turing mode is embedded in Hopf background that is oscillating in phase;
- (ii) Collapsed snaking: if the Turing mode is embedded in Hopf background that oscillates with a phase shift of π . This case corresponds to the “flip-flop” behaviour.

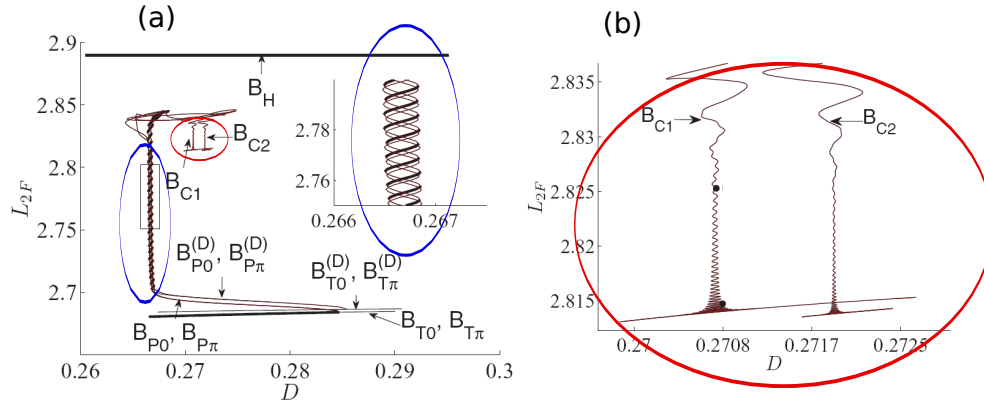


Figure 2.9:

(a) Complete bifurcation diagram of stationary solutions of the Brusselator model, with D as control parameter. In this case the norm is $L_{2f} \equiv \sqrt{\int_0^1 \sum_k [\hat{u}_k^2(t) + \hat{v}_k^2(t)] dt}$, where \hat{f}_k is the amplitude of the k th mode of the Fourier transform. Surrounded by blue circle is the vertical snaking branches, B_{P0} and $B_{P\pi}$. And in some way connected with this branches are two different branches B_{C1} and B_{C2} which present the collapsed snaking behaviour.

(b) Is shown a zoom to see more detail of the branches B_{C1} and B_{C2} in the collapsed snaking region. The solutions in this region correspond to the flip-flop behaviour.

Figures from [TMB⁺13].

Both cases form in the vicinity of a stationary front (Maxwell-type heteroclinic connection) between the Hopf (oscillatory) and the Turing (periodic) states, i.e., around $\gamma = \gamma_N$ in the context of

FCGL [see Eq. 2.62]. The width of the snaking regime is, however, rather narrow and depinning effects become dominant at small deviations from γ_N . Indeed, numerical integrations of (2.56) confirm this result also in the context of FCGL (see Fig. 2.10): for $\gamma > \gamma_N$ ($\gamma < \gamma_N$) the Turing (Hopf) state invades the Hopf (Turing) state [YEHM04b], and thus the localized Turing state (centered at $x = 0$) expands (collapses), respectively.

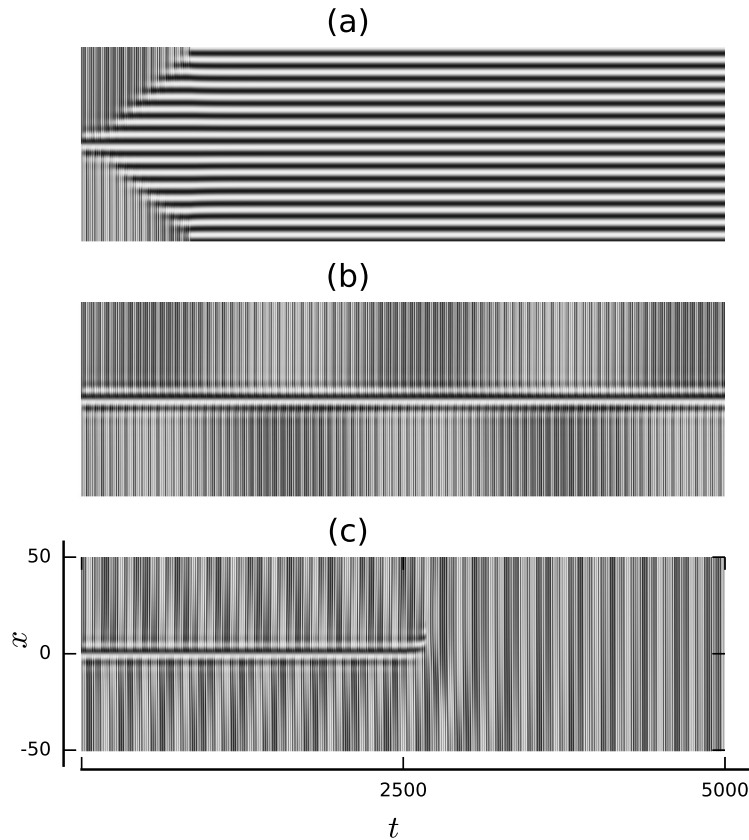


Figure 2.10: Direct numerical integration of (2.60) in 1D, showing the flip-flop and the depinning dynamics; light/dark colors indicate max/min value of the $u = \text{Re}(A)$ field, respectively. (a) $\gamma = 2.015 > \gamma_N \simeq 2.01$ (region II in Fig. 3.1), (b) $\gamma = \gamma_N \simeq 2.01$, (c) $\gamma = 2.002 < \gamma_N \simeq 2.01$ (region III in Fig. 3.1), while other parameters $\mu = 0.5$, $\nu = 2.2$, $\beta = 0$, $\alpha = 0.5$.

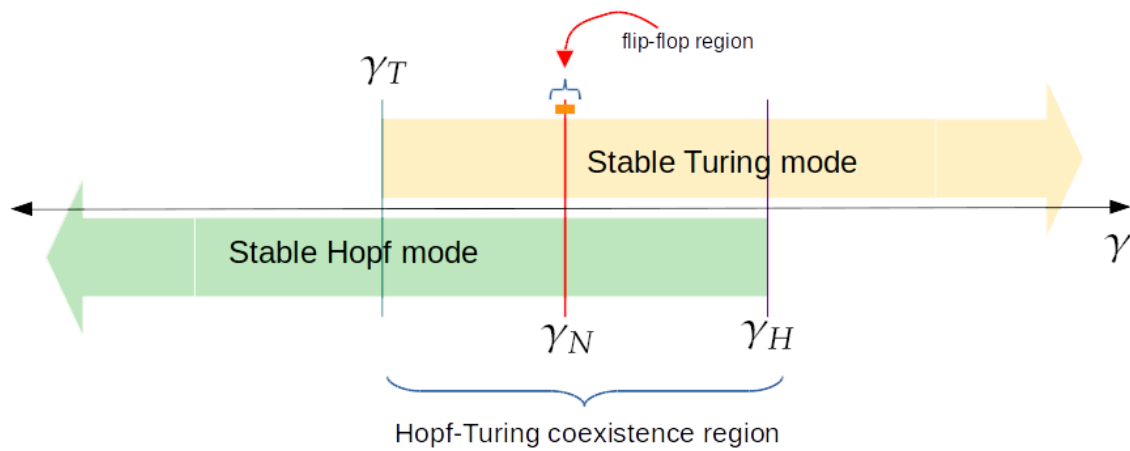


Figure 2.11: Schematic diagram that shows the stability regions of Hopf and Turing modes with γ as the control parameter. Also shows in a descriptive way the tiny region around γ_N , where flip-flop exists.

The reader should be careful with this diagram because it is not an accurate plot, in fact, for the sake of simplicity, we omit to show γ_b , the boundary of the resonance tongue. In this diagram it is assumed that $\gamma_b > \gamma_H$. But if γ_b were lesser than γ_H , then γ_b would be the upper limit of the stable Hopf mode, instead of γ_H .

Chapter 3

Research work

This chapter is meant to present the important aspects and results of the research project that we made with the collaboration and guidance of Dr. Arik Yochelis from Ben-Gurion University of the Negev. This section contains the main aspects that were published recently on April 2017 [MCY17]. The patterns of interest are the comb-like Turing patterns and the spiral waves with a Turing core, illustrated in Fig. 3.1(a). We use the Forced Complex Ginzburg-Landau (FCGL) equation (2.56). In previous studies, spiral waves with Turing core were related as a 2D extension of the flip-flop behaviour [DKPBE94, JPM⁺94]. In this work we show that the comb-like Turing pattern which is embedded in Hopf oscillations is generated by a different mechanism than flip-flop: the emergence of a Turing mode with a wave vector perpendicular to the Hopf front is the key of this comb-like pattern. In addition, we claim that the Turing core inside the Hopf spiral waves is formed by the same mechanism, which is consistent with the region of the parameter γ (forcing amplitude) where it appears, and also with the change of the size of the core with respect to this parameter. The physical relevance of this comb-like pattern is that it represents a structure where resonance 2:1 takes place (although only in a localized 2D domain) and this resonant behaviour occurs in a parameter region that is outside the hitherto known locking region.

This chapter is organized as follows: first we show how the parameter space is divided by different regions according to the resonant behaviour and the stability of the Hopf and Turing modes. In the previous section was shown the narrow parameter interval where 1D flip-flop is stable; now we introduce the comb-like Turing pattern embedded in a Hopf front within a 2D domain, and show numerically that these planar 2D comb-like localized states exist in a wide parameter range where flip-flop behavior is not present. Then, we present the corresponding amplitude equations obtained by a multiple scaling analysis, which takes into account three modes: Hopf mode, and two perpendicular Turing modes. Linear stability analysis is performed and also numerical integration of the amplitude equations. Then, in section 3.3, we exploit these insights to explain the comb-like spiral core; at the end, we show the results of the numerical integration of amplitude equations (with special attention on the amplitude corresponding to the Turing mode perpendicular to the front) are compared with the size of localized Turing patterns embedded in a Hopf front or spiral waves. Finally, we conclude in section 3.4.

3.1 Comb-like patterns and its parameter region

In this study, we focus on spatially localized comb-like structures in 2D, see for example Fig. 3.1(a). We show that these localized states emerge via an alternative pinning mechanism over a much wider range of parameters and specifically, in a region where 1D homoclinic snaking is absent. We exploit the context of frequency locking and show that the Hopf-Turing localization in 2D further extends the resonant behaviour outside of the resonance tongue [YHM⁺02, YEHM04b].

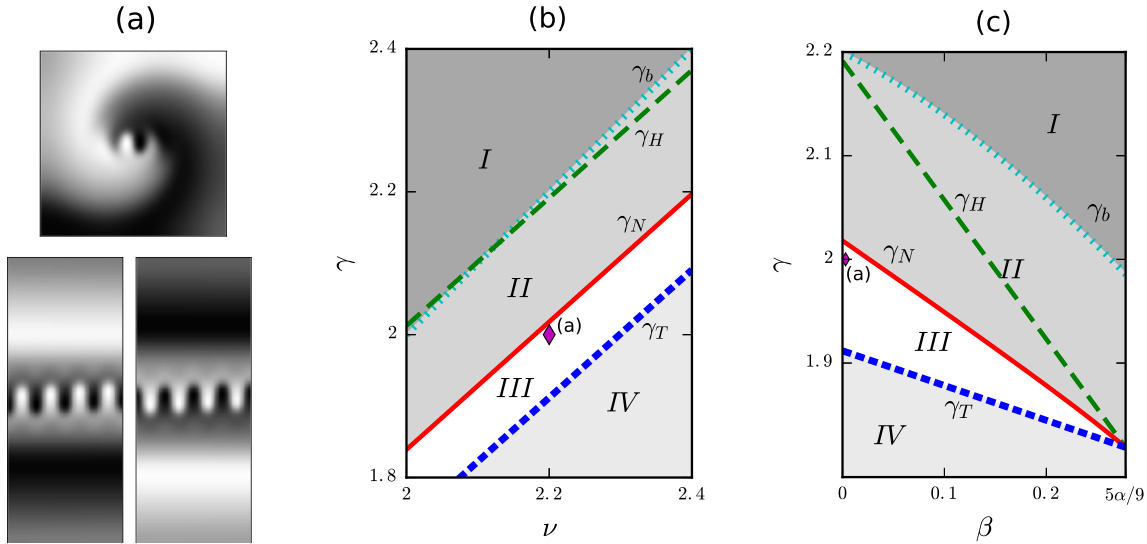


Figure 3.1: (a) Direct numerical integration of (2.56) in 2D, showing snapshots of comb-like localizations inside a spiral wave (top panel) and in between π shifted planar Hopf oscillations (bottom panel); light/dark colors indicate max/min value of the $Re(A)$ field, respectively. Neumann boundary conditions with no-flux were used on spatial domains of $x \in [0, 50]$, $y \in [0, 50]$ (top panel) and $x \in [0, 30]$, $y \in [0, 75]$ (bottom panel). (b) Applied forcing parameter plane (ν - γ) showing four distinct regions (see text for details and definitions): Region I, which is the classical 2:1 frequency locking region, $\gamma > \gamma_b$; Region II, in which frequency locking is extended due to dominance of Turing states, $\gamma_N \leq \gamma \leq \gamma_b$; Region III, in which Hopf states are dominant but localized comb-like Turing states can emerge (solutions such as presented in (a), with location indicated by (♦) symbol), $\gamma_T \leq \gamma \leq \gamma_N$; Region IV that supports only unlocked oscillations, $\gamma < \gamma_T$. (c) Parameter plane (β - γ) showing the limit ($\beta_c = 5\alpha/9$) of region III that corresponds to presence of pure Turing and Hopf modes (see text for details) while other symbols as in (b). Parameters: $\mu = 0.5$, $\alpha = 0.5$ and for (a) $\gamma = 2$, $\nu = 2.2$, $\beta = 0$.

3.2 Comb-like localized states

In this section, we show that localized comb-like states are formed due to pinning of a Turing mode that is perpendicular to the π phase shifted Hopf oscillations. Namely, we look for planar localized states, as shown in Figs. 3.2(d,e). At first, we derive the respective amplitude equations, then we obtain uniform solutions along with their stability properties, and finally confirm the results by direct numerical integrations. The numerical integration along this work was made with a finite differences method at first order approximation.

The robustness of comb-like structures (e.g., Fig. 3.1(a)) as compared to the narrow existence in the parameter space of the flip-flop, suggests that the emergence mechanism is distinct. Indeed, direct numerical simulations in 2D show that comb-like localized patterns emerge in a parameter range in which flip-flop ceases to exist $\gamma_T < \gamma < \tilde{\gamma}_N$, where $\tilde{\gamma}_N \lesssim \gamma_N$ is considered to be the left limit of the depinning region and computed here numerically, see Fig. 2.10. Notably, since the snaking region is very narrow as compared to the rest of the domain, we define in what follows region III to lie within $\gamma_T < \gamma < \gamma_N$. Moreover, the width (Γ) of the localized comb-like region increases with γ , as shown in Fig. 3.2. To quantify Γ , we employed a discrete Fourier transform (DFT) for every grid point. The dark shading marks the frequency with the highest contribution, as shown in the furthest right panels in Fig. 3.2. These results indeed confirm that comb-like states (see Fig. 3.1) are related to a distinct 2D pinning mechanism and not just a spatial extension of flip-flop dynamics [PDWD⁺93, Bha07, DWLDB96, JPM⁺94, MHM09].

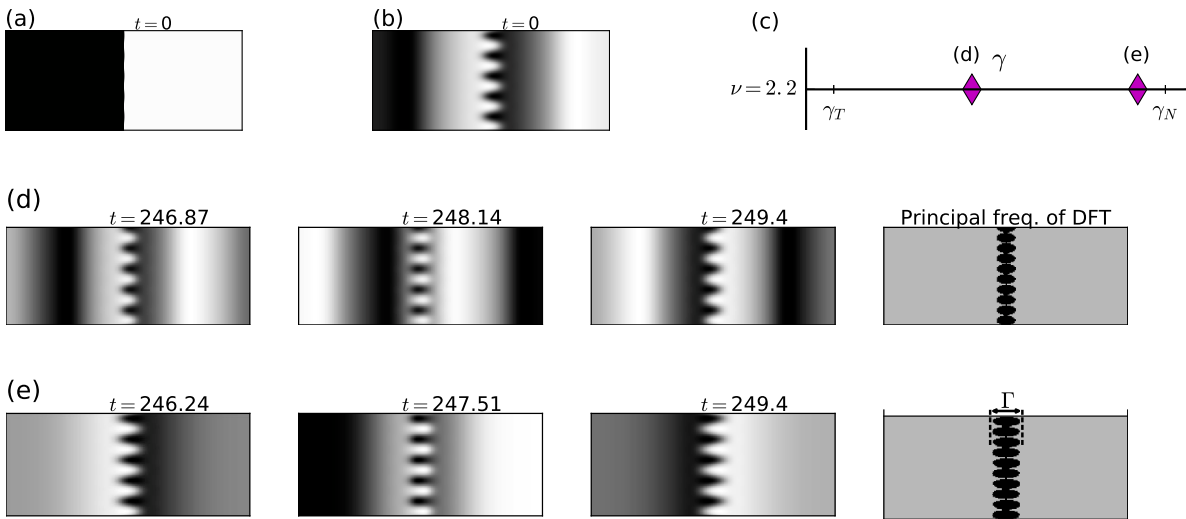


Figure 3.2: Direct numerical integration of (2.56) in 2D using (a) and (b) as initial conditions (at $t = 0$) for (d) $\gamma = 1.94$ and (e) $\gamma = 2$, respectively, as also indicated in top panel (c) by \blacklozenge symbols, respectively. The $Re(A)$ field is presented where light/dark colors indicate max/min values, respectively. The far right column, also with x and y axis, represents the frequencies with the highest amplitude obtained by discrete Fourier transform for the case (see text for details), respectively. Here, the gray color corresponds to $4/(\tau\Delta t)$, where $\tau = 40$ is the number of elements in the evaluated time series and $\Delta t = 0.633$ corresponds to time steps within the interval, thus, the time window length which was taken corresponds to $\tau(\Delta t) = 25.32$. The width of the comb-like state is then approximated by Γ which corresponds to the black color of vanishing amplitude value. The calculations were conducted on a spatial domain $x \in [0, 75]$, $y \in [0, 31.5]$, with no-flux boundary conditions in x and periodic in y . Parameters: $\mu = 0.5$. $\nu = 2.2$, $\beta = 0$, $\alpha = 0.5$. See moving frames at https://youtu.be/Uf0fq__9bYk.

Weakly nonlinear analysis

Derivation of amplitude equations in 2D follows, in fact the same steps as for the 1D case but with two Turing complex amplitudes (both varying slowly in space and time)

$$\begin{aligned} \begin{bmatrix} \text{Re}(A) \\ \text{Im}(A) \end{bmatrix} &\approx \begin{bmatrix} (1+i\alpha)/\rho \\ 1 \end{bmatrix} \tilde{H}(\sqrt{\epsilon}x, \sqrt{\epsilon}y, \epsilon t) e^{i\omega_c t} \\ &+ \begin{bmatrix} \alpha + \rho \\ 1 \end{bmatrix} \tilde{T}_{\parallel}(\sqrt{\epsilon}x, \sqrt{\epsilon}y, \epsilon t) e^{ik_c x} \\ &+ \begin{bmatrix} \alpha + \rho \\ 1 \end{bmatrix} \tilde{T}_{\perp}(\sqrt{\epsilon}x, \sqrt{\epsilon}y, \epsilon t) e^{ik_c y} \\ &+ c.c., \end{aligned} \quad (3.1)$$

The two Turing modes \tilde{T}_{\parallel} and \tilde{T}_{\perp} are explicit function of the slow variables and are defined as parallel and perpendicular to the considered π phase shifted Hopf oscillations (hereafter, Hopf front), respectively. Following the multiple time scale method (see [YEHM04b] for details), we obtain (after some algebra that is shown in the Appendix)

$$\begin{aligned} \frac{\partial H}{\partial t} &= m_1 H - m_2 |H|^2 H - m_3 (|T_{\perp}|^2 + |T_{\parallel}|^2) H \\ &+ m_4 \nabla^2 H, \end{aligned} \quad (3.2a)$$

$$\begin{aligned} \frac{\partial T_{\parallel}}{\partial t} &= n_1 T_{\parallel} - n_2 (|T_{\parallel}|^2 + 2|T_{\perp}|^2) T_{\parallel} - n_3 |H|^2 T_{\parallel} \\ &+ n_4 \frac{\partial^2 T_{\parallel}}{\partial x^2}, \end{aligned} \quad (3.2b)$$

$$\begin{aligned} \frac{\partial T_{\perp}}{\partial t} &= n_1 T_{\perp} - n_2 (2|T_{\parallel}|^2 + |T_{\perp}|^2) T_{\perp} - n_3 |H|^2 T_{\perp} \\ &+ n_4 \frac{\partial^2 T_{\perp}}{\partial y^2}. \end{aligned} \quad (3.2c)$$

Besides the standard Hopf-Turing solutions [YEHM04b], uniform solutions to (3.2) that involve non-vanishing T_{\perp} contributions, are obtained through the amplitudes $(|H|, |T_{\parallel}|, |T_{\perp}|) := (R_H, R_{\parallel}, R_{\perp}) = (\tilde{R}_H, \tilde{R}_{\parallel}, \tilde{R}_{\perp})$:

(i) Pure Turing modes (stripes),

$$\tilde{R}_{\perp} = \sqrt{\frac{\mu\alpha + \rho(\gamma - \gamma_c)}{6\rho(\alpha + \rho)(\alpha - \beta)}}, \quad \tilde{R}_H = \tilde{R}_{\parallel} = 0; \quad (3.3)$$

(ii) Unstable mixed Turing mode (stationary squares),

$$\tilde{R}_{\perp} = \tilde{R}_{\parallel} = \sqrt{\frac{\mu\alpha + \rho(\gamma - \gamma_c)}{18\rho(\alpha + \rho)(\alpha - \beta)}}, \quad \tilde{R}_H = 0; \quad (3.4)$$

(iii) Unstable mixed Hopf-Turing mode (oscillating squares),

$$\begin{aligned}\tilde{R}_H &= \frac{1}{2} \sqrt{\frac{(18\beta - 2\alpha)\mu + 16\rho(\gamma - \gamma_c)}{14\alpha - 30\beta}}, \\ \tilde{R}_\perp = \tilde{R}_\parallel &= \sqrt{\frac{(\alpha - 3\beta)\mu - \rho(\gamma - \gamma_c)}{\rho(\alpha + \rho)(14\alpha - 30\beta)}}.\end{aligned}\quad (3.5)$$

Stability and Hopf fronts

After obtaining uniform solutions, we proceed to the selection mechanism by focusing on the spatial symmetry breaking that is induced by the Hopf front. Consequently, we associate (3.2) with only one spatial dependence (here we use x), which corresponds to the direction of a Hopf front. In addition, for convenience we use polar form $H = R_H \exp(i\Phi)$ and consider only the amplitudes of Turing fields (spatial dependence H cannot be decoupled as for $T_{\parallel,\perp}$). Hence, system (3.2) becomes

$$\begin{aligned}\frac{\partial R_H}{\partial t} &= \mu R_H - 4R_H^3 - 8\rho(\alpha + \rho)(R_\parallel^2 + R_\perp^2)R_H \\ &\quad - \left[\left(\frac{\partial \Phi}{\partial x} \right)^2 + \rho \frac{\partial^2 \Phi}{\partial x^2} \right] R_H - 2 \frac{\partial \Phi}{\partial x} \frac{\partial R_H}{\partial x}, \\ &\quad + \frac{\partial^2 R_H}{\partial x^2}\end{aligned}\quad (3.6a)$$

$$\begin{aligned}\frac{\partial \Phi}{\partial t} &= -\frac{\gamma - \gamma_c}{\alpha} - \nu_1 R_H^2 - \nu_2 (R_\parallel^2 + R_\perp^2) \\ &\quad - \left[\rho \left(\frac{\partial \Phi}{\partial x} \right)^2 - \frac{\partial^2 \Phi}{\partial x^2} \right] + \frac{2}{R_H} \frac{\partial \Phi}{\partial x} \frac{\partial R_H}{\partial x} \\ &\quad + \frac{\rho}{R_H} \frac{\partial^2 R_H}{\partial x^2},\end{aligned}\quad (3.6b)$$

$$\begin{aligned}\frac{\partial R_\parallel}{\partial t} &= \left[\mu + \frac{\rho(\gamma - \gamma_c)}{\alpha} \right] R_\parallel - 4 \left(2 - 3 \frac{\beta}{\alpha} \right) R_H^2 R_\parallel \\ &\quad - 6\rho(\alpha + \rho) \left(1 - \frac{\beta}{\alpha} \right) (R_\parallel^2 + 2R_\perp^2) R_\parallel \\ &\quad + 2\rho^2 \frac{\partial^2 R_\parallel}{\partial x^2},\end{aligned}\quad (3.6c)$$

$$\begin{aligned}\frac{\partial R_\perp}{\partial t} &= \left[\mu + \frac{\rho(\gamma - \gamma_c)}{\alpha} \right] R_\perp - 4 \left(2 - 3 \frac{\beta}{\alpha} \right) R_H^2 R_\perp \\ &\quad - 6\rho(\alpha + \rho) \left(1 - \frac{\beta}{\alpha} \right) (2R_\parallel^2 + R_\perp^2) R_\perp,\end{aligned}\quad (3.6d)$$

where $\nu_1 = 2\beta(2\rho^2 + 1)/(\alpha\rho)$, and $\nu_2 = 4\beta[2\alpha\rho(\alpha + \rho) + 3\rho + \alpha]/\alpha - 4(\alpha + \rho)$. Notably, the spatial symmetry breaking is reflected in (3.6d) through the absence of a diffusive term.

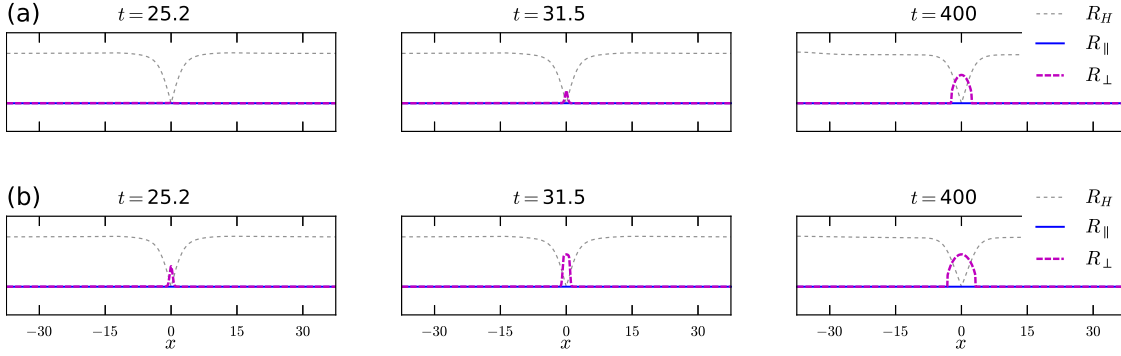


Figure 3.3: Direct numerical integration of (3.2) showing snapshots of the amplitudes $(R_H, R_{\parallel}, R_{\perp})$ at (a) $\gamma = 1.94$ and (b) $\gamma = 2$ (as also indicated in Fig. 3.2(c)). The calculations were conducted on a 1D spatial domain $x \in [0, 75]$, under no-flux boundary conditions, and parameters: $\mu = 0.5$, $\nu = 2.2$, $\beta = 0$, $\alpha = 0.5$. See moving frames at <https://youtu.be/pEYVGSi9jZM>.

The fixed point analysis (linear stability to spatially uniform perturbations) of (3.6) is identical to the standard Hopf-Turing analysis [YEHM04b], and thus, the pure Hopf and pure Turing coexistence regime remains the same, $\beta < 5\alpha/9$. However, to gain insights into the emergence of the T_{\perp} mode at the Hopf front region, we examine the linear stability of the trivial solution $(\tilde{R}_H, \tilde{R}_{\parallel}, \tilde{R}_{\perp})^T = (0, 0, 0)^T$ to non-uniform perturbations, for which the Hopf amplitude and phase can be decoupled:

$$\begin{pmatrix} R_H \\ R_{\parallel} \\ R_{\perp} \end{pmatrix} - \begin{pmatrix} \tilde{R}_H \\ \tilde{R}_{\parallel} \\ \tilde{R}_{\perp} \end{pmatrix} \propto e^{\sigma t - ikx} + c.c., \quad (3.7)$$

which mean that the absolute value of the difference between the state $(R_H, R_{\parallel}, R_{\perp})^T$ and the stationary solution $(\tilde{R}_H, \tilde{R}_{\parallel}, \tilde{R}_{\perp})^T$ will be a vector that grow or decay exponentially and oscillates in space with the k -mode; where σ is the growth rate that correspond to the wavenumber k . Substitution of (3.7) in (3.6) and solving to a leading order, yields three dispersion relations:

$$\sigma_H = \mu - k^2, \quad (3.8)$$

$$\sigma_0 = \mu + \rho \frac{\gamma - \gamma_c}{\alpha}. \quad (3.9)$$

$$\sigma_k = \mu + \rho \frac{\gamma - \gamma_c}{\alpha} - 2\rho^2 k^2. \quad (3.10)$$

As expected, the three growth rates show instability for $k = 0$, where the vector flow is rather isotropic (Fig. 3.4). For completeness, we have computed the trajectories after linearizing (3.6) about all the fixed points with $R_H = 0$, and show them on the $(R_{\parallel}, R_{\perp})$ plane. The results are consistent with the stability of pure Turing modes (3.3) and the saddle for a mixed Turing mode (3.4). As k is increased, we observe a symmetry breaking between σ_0 and σ_k , which occurs for $\sigma_k = 0$ or equivalently for

$$k_f^2 = \frac{\mu\alpha + \gamma\rho - \nu}{2\rho^2}. \quad (3.11)$$

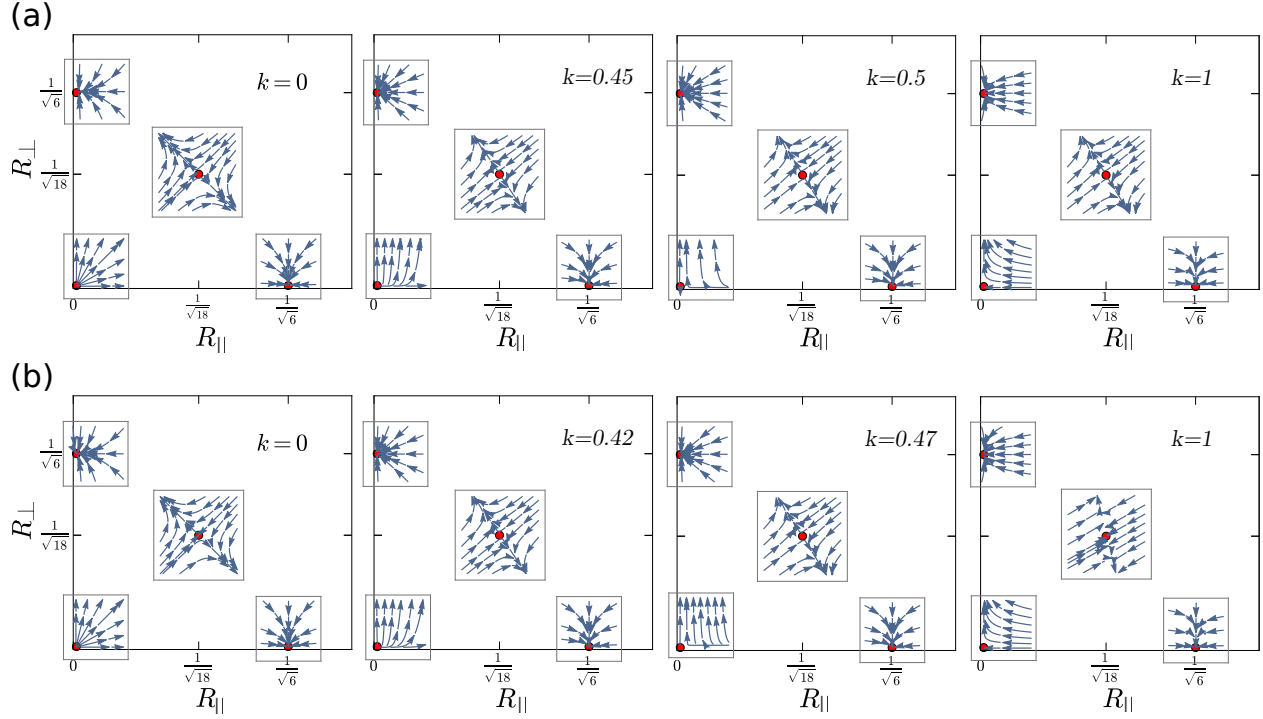


Figure 3.4: Streamline of linearized vector flow for (3.6) about four fixed points at (a) $\gamma = 1.94$ and (b) $\gamma = 2$, plotted on the $(R_{\parallel}, R_{\perp})$ plane, and calculated for four distinct wavenumbers, as shown from left to right: $k \rightarrow 0$, $k \lesssim k_f$, $k \gtrsim k_f$, and $k > k_f$, where k_f is given in (3.11). The axis units are $\sqrt{6}\tilde{R}_{\parallel, \perp}$ according to (3.3), and parameters: $\mu = 0.5$, $\nu = 2.2$, $\beta = 0$, $\alpha = 0.5$.

Figure 3.4 shows that the perturbations about $(R_{\parallel}, R_{\perp}) = (0, 0)$ favor the attractor $(R_{\parallel}, R_{\perp}) = (0, \tilde{R}_{\perp})$. The increasing value of the wavenumber is also consistent with the basin of attraction which corresponds to a rather narrow spatial region due to the Hopf front location, i.e., already for $k = 1$ the flow indicates ultimate preference toward $(R_{\parallel}, R_{\perp}) = (0, \tilde{R}_{\perp})$.

Numerical results

Next, we check the above obtained results vs. direct numerical integrations of (3.2). We set a sharp Hopf front by using the Hopf amplitude as an initial condition: $R_H(x = 0 \dots \pm L) = \mp \tilde{R}_H$ and $R_{\parallel} = R_{\perp} = 0$. Due to diffusion in the Hopf field, at first a front solution is indeed formed and after additional transient, an asymptotic localized T_{\perp} Turing state emerges inside the Hopf front region, as shown in Fig. 3.3. The results are in accord with the linear stability analysis of the trivial state, showing that perturbations at the mid front location $x = 0$, are in the basin of attraction of the fix point $(R_H, R_{\parallel}, R_{\perp}) = (0, 0, \tilde{R}_{\perp})$ which corresponds to the comb-like structure in Fig. 3.2. The width of the T_{\perp} Turing localized state increases with γ , which agrees well with numerical integration of (2.56), as shown in Fig. 3.5. This could be an important feature that explains the different size of Turing core embedded in spiral waves. We note that in the narrow vicinity of

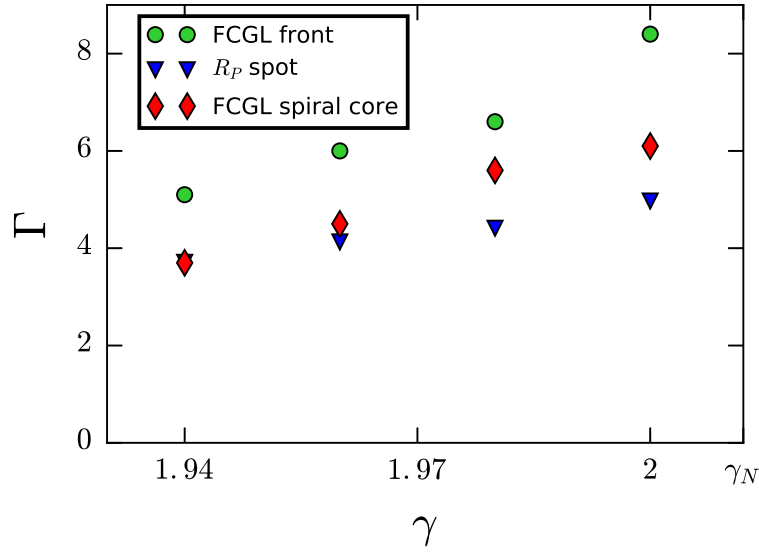


Figure 3.5: Width (Γ) of the comb-like state as obtained from direct numerical integrations of (2.56) in two space dimensions, and a localized T_{\perp} Turing state using (3.2). Parameters: $\mu = 0.5$, $\nu = 2.2$, $\beta = 0$, $\alpha = 0.5$. Notably, although μ is about order 1 from the co-dimension 2 onset ($\mu = 0$), the width of T_{\perp} obtained from integration of (3.2) is well within the range of comb-like solutions to (2.56).

γ_N both Turing modes, T_{\perp} and T_{\parallel} , coexist and can emerge depending on the initial perturbations within the Hopf front.

The Turing mode that is parallel to the Hopf front (T_{\parallel}) is being described by a partial differential equation (3.6c) and thus in the absence of a pinning mechanism such as, homoclinic snaking, is being directly subjected to diffusive fluxes, which are overtaken by the oscillatory Hopf mode. On the other hand, the perpendicular Turing mode (T_{\perp}) obeys only a local dynamics via an ordinary differential equation (3.6d). The spatial decoupling in (3.6d) allows thus, under certain initial conditions, pinning of the Hopf amplitude (local selection of the $(R_H, R_{\parallel}, R_{\perp}) = (0, 0, \tilde{R}_{\perp})$ fixed point), which in turn results effectively in a π phase shifted front. This, however, is sensitive to domain size or initial conditions due to the secondary zig-zag and Eckhaus instabilities [CH93, Mer15]. For example, the length of y dimension should be an integer of the typical wavenumber which is close to k_c and within the Eckhaus stable regime; details of the Busse balloon for this problem are given in [YEHM04b]. If this condition is not fulfilled, the nonlinear terms become dominant and the comb-like structures are destroyed and instead a spiral wave with a comb-like core is formed, see Fig. 3.6.

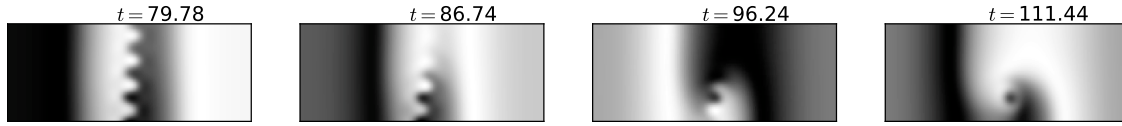


Figure 3.6: Direct numerical integration of (2.56) in 2D, showing snapshots of the $Re(A)$ field for $\gamma = 1.94 < \gamma_N$; light/dark colors indicate max/min values, respectively. Initial condition was the same illustrated in Fig. 3.2(a). The calculations were conducted on a spatial domain $x \in [0, 75]$, $y \in [0, 30]$ with no-flux boundary conditions. Other parameters: $\mu = 0.5$, $\nu = 2.2$, $\beta = 0$, $\alpha = 0.5$.

3.3 Spiral waves with comb-like core

To capture the emergence of the Turing core embedded inside a Hopf spiral, we start with a pure Hopf spiral wave obtained for $\gamma = 1.9$, as an initial condition. As for the planar front case (Fig. 3.2), direct numerical integration of (2.56) for $\gamma_T < \gamma < \gamma_N$ shows formation of a Turing spot inside the core due to the vanishing amplitude of the Hopf amplitude within that region, see Fig. 3.7. As expected, also here, the Turing core size increases with γ .

To quantify the size of the Turing core, we use again DFT for each grid point within a window of 128 time steps, where each time step is made out of 100 discrete time iterations. Consequently, each grid point corresponds to a 128-dimensional vector with the amplitude calculated from DFT, where only the elements with the highest amplitude value are selected, as shown in the bottom panel of Fig. 3.7. The frequency contrast allows us to define a criterion for the width (Γ) of the Turing spot. The spiral core width is found to agree with results obtained via the planar front initial condition, as shown Fig. 3.5. In the depinning region above the stationary Hopf-Turing front condition $\gamma_N < \gamma < \gamma_b$, the spiral core expands by invasion into the Hopf oscillations due to the dominance of the Turing mode and the domain is filled with a periodic pattern [YHM⁺02] (not shown here).

3.4 Conclusions

In summary, we have presented a distinct pinning mechanism for 2D spatial localization that is associated with the emergence of *comb-like* structures embedded in a temporally oscillatory background. These spatially localized states emerge in a planar form inside π phase shift oscillations (Fig. 3.2) or as a spiral wave core (Fig. 3.7). The mechanism requires coexistence of periodic stripes in both x and y directions and uniform oscillations, a behavior that is typical in the vicinity of a codimension-2 Hopf-Turing bifurcation. Unlike the homoclinic snaking mechanism that gives rise to localized states over a narrow range of parameters about a stationary Hopf-Turing front in 1D (a.k.a. flip-flop dynamics) [TMB⁺13], the comb-like states are robust (i.e., do not require any Maxwell type construction) and exist over the entire coexistence range even though the Hopf state is dominant over the Turing ($\gamma_T < \gamma < \gamma_N$), as shown in Figs. 3.1 and 3.5.

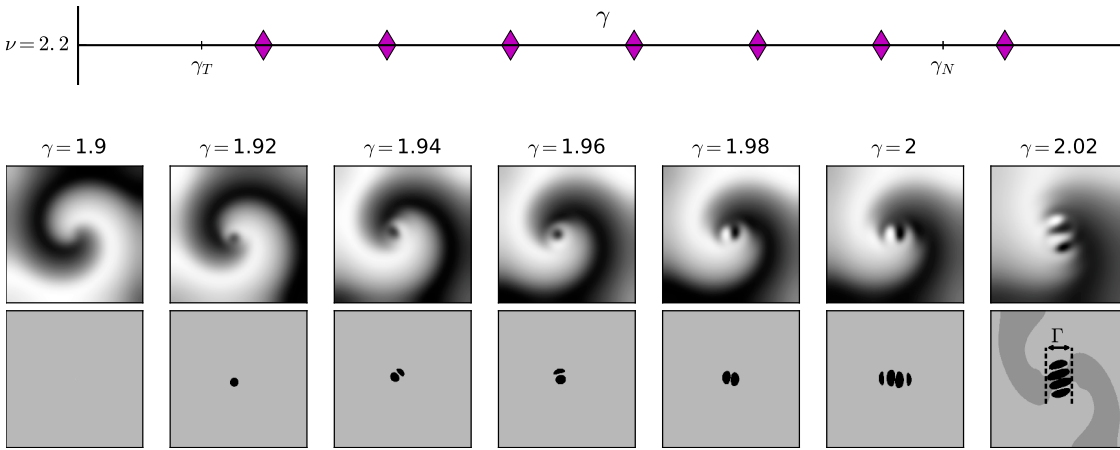


Figure 3.7: Direct numerical integration of (2.56) in 2D, showing snapshots of the $Re(A)$ field for various values of γ as indicated for each frame in the middle panel and also indicated in top panel by (\blacklozenge) symbols, respectively; light/dark colors indicate max/min values, respectively. Bottom panel represents the frequencies with highest amplitude obtained by discrete Fourier transform for the case in the middle panel (see text and Fig. 3.2 for details), respectively. The calculations were conducted on a spatial domain $x \in [0, 50]$, $y \in [0, 50]$ with no-flux boundary conditions. Parameters: $\mu = 0.5$, $\nu = 2.2$, $\beta = 0$, $\alpha = 0.5$. See moving frames at <https://youtu.be/DsuJLwP9B4k>.

In the context of 2:1 frequency locking, the comb-like states correspond to spatially localized resonances that further extend the frequency locking regime outside the resonance tongue. Notably, localized comb-like states have been also observed in vibrating granular media and referred to as “decorated fronts” [BAC⁺00]. However, in these experiments they seem to form near resonant domain patterns and thus, their formation mechanisms may be unrelated to the Hopf-Turing bifurcation.

To this end, using the generic amplitude equation framework, we have presented a selection mechanism that allows us to understand and robustly design spatially localized reaction-diffusion patterns in two dimensional geometries [VE08, DBDW⁺95, BJP⁺95]. Specifically, these results indicate the origin of intriguing spiral waves with stationary cores that have been observed in CIMA chemical reaction [DKPBE94, JPM⁺94] and suggest the formation of localized resonant patterns outside the classical 2:1 frequency locking region, as such in the case of periodically driven Belousov-Zhabotinski chemical reaction [YHM⁺02]. A detailed analysis/comparison with reaction-diffusion models for chemical reactions is however, beyond the scope of this work and should be addressed in future studies.

Chapter 4

Appendix

.1 Multiple scales and weakly non-linear analysis

The codimension-2 Hopf-Turing instability bifurcation is located at $\mu = 0$ and $\gamma = \gamma_c$; to facilitate calculations we will use the auxiliary parameter $\tilde{d} = d/\mu$, where $d = (\gamma - \gamma_c)$. Near de codimension-2 point bifurcation, the solution at first approximation takes into account only a single frequency ω_c in time and a wavenumber k_c for oscillations in space; but we will consider exclusively two perpendicular Turing modes, in x and y direction:

$$\begin{bmatrix} u_0 \\ v_0 \end{bmatrix} = \begin{bmatrix} c \\ 1 \end{bmatrix} B_H e^{i\omega_c t} + \begin{bmatrix} \eta \\ 1 \end{bmatrix} B_X e^{ik_c x} + \begin{bmatrix} \eta \\ 1 \end{bmatrix} B_Y e^{ik_c y} + c.c., \quad (1)$$

where the amplitudes B_H , B_X and B_Y are not constant, but depend on slow variables $T = \mu t$, $X = \sqrt{\mu}x$ and $Y = \sqrt{\mu}y$, which describes just weak modulations of the periodic pattern.

FCGL solution can be expanded:

$$\begin{bmatrix} u \\ v \end{bmatrix} = \sqrt{\mu} \begin{bmatrix} u_0 \\ v_0 \end{bmatrix} + \mu \begin{bmatrix} u_1 \\ v_1 \end{bmatrix} + \mu^{3/2} \begin{bmatrix} u_2 \\ v_2 \end{bmatrix} + \dots \quad (2)$$

Placing (2) in eq.(2.60), where $u = \text{Re}(A)$ and $v = \text{Im}(A)$, we obtain three differential equations corresponding to $\sqrt{\mu}$, μ and $\mu^{3/2}$ order. For each equation we have to impose the solvability conditions in order to avoid resonant terms; this imposition leads to equations of the amplitudes $B_H(T, X, Y)$, $B_X(X, Y, T)$, $B_Y(X, Y, T)$. Finally, the equations are rescaled back to the fast time and space variables, to obtain the amplitude equations desired.

After expansion (2) is needed to substitute it into FCGL equation (2.56) for real and imaginary part. But the expansion terms u_i and v_i (for $i = 0, 1, 2$) explicitly depend on normal and slow variables, which has to be taken into account in the derivative operators by carefully applying the chain

rule; or, equivalently, to make the following substitution in the equation:

$$\begin{aligned} \frac{\partial}{\partial t} &\rightarrow \frac{\partial}{\partial t} + \mu \frac{\partial}{\partial T}, \\ \frac{\partial}{\partial x} &\rightarrow \frac{\partial}{\partial x} + \sqrt{\mu} \frac{\partial}{\partial X}, \quad \frac{\partial}{\partial y} \rightarrow \frac{\partial}{\partial y} + \sqrt{\mu} \frac{\partial}{\partial Y}, \end{aligned} \quad (3)$$

then will be obtain three non linear equation of $[u_i, v_i]$ for each order $i = 0, 1, 2$, of the form:

$$\mathcal{M} \begin{bmatrix} u_0 \\ v_0 \end{bmatrix} = |R_0\rangle, \quad (4)$$

$$\mathcal{M} \begin{bmatrix} u_1 \\ v_1 \end{bmatrix} = |R_1\rangle, \quad (5)$$

$$\mathcal{M} \begin{bmatrix} u_2 \\ v_2 \end{bmatrix} = |R_2\rangle, \quad (6)$$

where \mathcal{M} is a linear operator and $|R_i\rangle$ is a two-dimensional vector column that depends on lower order contributions of the solution. In this case the operator is:

$$\mathcal{M} = \begin{bmatrix} \gamma_c + \nabla^2 - \partial_t & -\nu - \alpha \nabla^2 \\ \nu + \alpha \nabla^2 & -\gamma_c + \nabla^2 - \partial_t \end{bmatrix}.$$

And the equations up to the 3/2 order get the following form.

For $\sqrt{\mu}$ order:

$$\mathcal{M} \begin{bmatrix} u_0 \\ v_0 \end{bmatrix} = \begin{bmatrix} 0 \\ 0 \end{bmatrix} \equiv |R_0\rangle. \quad (7)$$

For μ order:

$$\mathcal{M} \begin{bmatrix} u_1 \\ v_1 \end{bmatrix} = -\mathcal{L}_1 \begin{bmatrix} u_0 \\ v_0 \end{bmatrix} \equiv |R_1\rangle, \quad (8)$$

where $\mathcal{L}_1 \equiv 2(\partial_X \partial_x + \partial_Y \partial_y) \begin{bmatrix} 1 & -\alpha \\ \alpha & 1 \end{bmatrix}$.

For $\mu^{3/2}$ order:

$$\mathcal{M} \begin{bmatrix} u_2 \\ v_2 \end{bmatrix} = -\mathcal{L}_1 \begin{bmatrix} u_1 \\ v_1 \end{bmatrix} - \mathcal{L}_0 \begin{bmatrix} u_0 \\ v_0 \end{bmatrix} + \mathcal{N}_0 \begin{bmatrix} u_0 \\ v_0 \end{bmatrix} \equiv |R_2\rangle, \quad (9)$$

$$\text{where } \mathcal{L}_0 \equiv \begin{bmatrix} 1 + \tilde{d} + \nabla_{[X,Y]}^2 - \partial_t & -\alpha \nabla_{[X,Y]}^2 \\ \alpha \nabla_{[X,Y]}^2 & 1 - \tilde{d} + \nabla_{[X,Y]}^2 - \partial_t \end{bmatrix}, \quad \text{and} \quad \mathcal{N}_0 \equiv (u_0^2 + v_0^2) \begin{bmatrix} 1 & -\beta \\ \beta & 1 \end{bmatrix},$$

whith $\nabla_{[X,Y]}^2 \equiv \partial_X^2 + \partial_Y^2$.

$\begin{bmatrix} u_0 \\ v_0 \end{bmatrix}$ is solution of eq. (7) and it is needed to specify $|R_1\rangle$. In the same manner $\begin{bmatrix} u_1 \\ v_1 \end{bmatrix}$ is solution of the following order equation (8) and, along with explicit form of $\begin{bmatrix} u_0 \\ v_0 \end{bmatrix}$, it is needed to specify $|R_2\rangle$.

To solve equation (7) we can take as guess two solutions, the former consists in Hopf-mode (oscillations in time): $\begin{bmatrix} u_0 \\ v_0 \end{bmatrix}_t = \begin{bmatrix} c \\ 1 \end{bmatrix} e^{i\omega_c t}$, and the latter is in Turing-mode (oscillations in space whose direction is specified by φ): $\begin{bmatrix} u_0 \\ v_0 \end{bmatrix}_\varphi = \begin{bmatrix} \eta \\ 1 \end{bmatrix} e^{ik_c(\cos \varphi x + \sin \varphi y)}$, where c and η are constant that will specify the direction of the solution vector.

Because of linearity of equation (4), any linear combination is also a solution. So as general solution we have:

$$\begin{aligned} \begin{bmatrix} u_0 \\ v_0 \end{bmatrix} &= B_t \begin{bmatrix} (1 + i\alpha)/\rho \\ 1 \end{bmatrix} e^{i\omega_c t} \\ &+ \begin{bmatrix} \alpha + \rho \\ 1 \end{bmatrix} \int_0^\pi B_\varphi e^{ik_c(\cos \varphi x + \sin \varphi y)} d\varphi + c.c. \end{aligned} \quad (10)$$

B_t and B_φ are undetermined coefficients. The complex conjugate (c.c.) is added to give only real solutions and integral takes into account all the possible direction of Turing modes.

But in the present work we are going to be only concern on two perpendicular Turing modes ($\varphi = 0$ and $\varphi = \pi/2$):

$$\begin{bmatrix} u_0 \\ v_0 \end{bmatrix} = \begin{bmatrix} c \\ 1 \end{bmatrix} B_H e^{i\omega_c t} + \begin{bmatrix} \eta \\ 1 \end{bmatrix} B_X e^{ik_c x} + \begin{bmatrix} \eta \\ 1 \end{bmatrix} B_Y e^{ik_c y} + c.c.. \quad (11)$$

Let us remind the value of some important quantities in terms of the parameters of the FCGL equation (2.56):

$$\begin{aligned} \omega_c &= \nu\alpha/\rho, & \gamma_c &= \nu/\rho, & \eta &= \alpha + \rho, \\ k_c^2 &= \nu\alpha/\rho^2, & c &= (1 + i\alpha)/\rho, & \rho &= \sqrt{1 + \alpha^2}. \end{aligned}$$

In the Appendix .3 some useful equations and identities are presented.

What follows is to obtain the explicit form of $|R_1\rangle$ and $|R_2\rangle$. First, with explicit solution $\begin{bmatrix} u_0 \\ v_0 \end{bmatrix}$ we get $|R_1\rangle$, and solving differential equation (5) we will get $\begin{bmatrix} u_1 \\ v_1 \end{bmatrix}$ which is needed for explicit expression of $|R_2\rangle$.

For each $|R_j\rangle$ that we get, we have to ensure that $|R_j\rangle$ fulfills its respective solvability condition, that will be explained in the following. At the end, solvability conditions corresponding to $|R_2\rangle$ will give the amplitude equations that we are looking for.

Equations (4-6) can be written as

$$\mathcal{M}|u_j\rangle = |R_j\rangle, \quad (12)$$

where $|u_j\rangle = \begin{bmatrix} u_j \\ v_j \end{bmatrix}$, for $j = 0, 1, 2$.

Since we take into account the coexistence of only three modes, an arbitrary periodic and bounded vector $|w\rangle$ will be a series of trigonometrical polynomials of the form:

$$|w\rangle = \sum_n \sum_m \sum_p \begin{bmatrix} a_{nmp} \\ b_{nmp} \end{bmatrix} e^{ni\omega_c t} e^{ik_c(mx+py)}.$$

The null space of \mathcal{M} has dimension three, and it is generated by the following vectors, see (11):

$$\begin{bmatrix} c \\ 1 \end{bmatrix} e^{i\omega_c t}, \quad \begin{bmatrix} \eta \\ 1 \end{bmatrix} e^{ik_c x}, \quad , \quad \begin{bmatrix} \eta \\ 1 \end{bmatrix} e^{ik_c y}.$$

It is easy to find coefficient vectors that are orthogonal for the null space of each mode: $\begin{bmatrix} 1 \\ -c^* \end{bmatrix}$, $\begin{bmatrix} 1 \\ -\eta \end{bmatrix}$ and $\begin{bmatrix} 1 \\ -\eta \end{bmatrix}$, respectively.

Let us get the vectors $|f_t\rangle$, $|f_x\rangle$ and $|f_y\rangle$ that generate the image for each mode:

$$\mathcal{M} \begin{bmatrix} 1 \\ -c^* \end{bmatrix} e^{i\omega_c t} = 2\nu \begin{bmatrix} c^* \\ 1 \end{bmatrix} e^{i\omega_c t}, \quad (13)$$

$$\mathcal{M} \begin{bmatrix} 1 \\ -\eta \end{bmatrix} e^{ik_c x} = \frac{2\nu}{\rho} \begin{bmatrix} 1 \\ \alpha + \rho \end{bmatrix} e^{ik_c x}. \quad (14)$$

Then we have: $|g_t\rangle = \begin{bmatrix} c^* \\ 1 \end{bmatrix}$, $|g_x\rangle = |g_y\rangle = \begin{bmatrix} 1 \\ \alpha + \rho \end{bmatrix}$, and the first order polynomial trigonometric terms of the image are generated by:

$$|g_t\rangle e^{i\omega_c t}, \quad |g_x\rangle e^{ik_c x}, \quad |g_y\rangle e^{ik_c y}, \quad (15)$$

and it can be verified that the following vectors are orthogonal to each of the vectors $|g_t\rangle, |g_x\rangle$ and $|g_y\rangle$, respectively:

$$|h_t\rangle = \begin{bmatrix} -c^* \\ 1 \end{bmatrix}, \quad |h_x\rangle = |h_y\rangle = \begin{bmatrix} 1 \\ \alpha - \rho \end{bmatrix}, \quad \text{with } c^* = \frac{1 - i\alpha}{\rho}.$$

$|R_0\rangle = \begin{bmatrix} 0 \\ 0 \end{bmatrix}$, so there is no need to impose a solvability condition.

Now let's get explicit form of $|R_1\rangle$. Then we can solve eq. (5).

Substituting (11) in (8) we have:

$$|R_1\rangle = -2ik_c \left[(\partial_X B_X) e^{ik_c x} + (\partial_Y B_Y) e^{ik_c y} \right] \begin{bmatrix} \rho \\ \alpha\eta + 1 \end{bmatrix} + \text{c.c.} \quad (16)$$

It is easily seen that $\begin{bmatrix} \rho \\ \alpha\eta + 1 \end{bmatrix} = \rho \begin{bmatrix} 1 \\ \alpha + \rho \end{bmatrix} = \rho |g_x\rangle = \rho |g_y\rangle$, thus $|R_1\rangle$ already belongs to the image of \mathcal{M} .

Now that we have $|R_1\rangle$, we can solve the equation (5). As both elements of $|R_1\rangle$ are not explicitly dependent on t , only on $e^{ik_c x}$ and $e^{ik_c y}$ (and its respective complex conjugate), then the guess solution will only have dependence on those exponential.

As particular solution of the equation (5) is proposed the following:

$$\begin{bmatrix} u_1 \\ v_1 \end{bmatrix}_p = \begin{bmatrix} a_1 \\ a_2 \end{bmatrix} (ik_c \partial_X B_X) e^{ik_c x} + \begin{bmatrix} b_1 \\ b_2 \end{bmatrix} (ik_c \partial_Y B_Y) e^{ik_c y} + \text{c.c.}$$

Testing it in the left side of equation (5) we get infinite solutions for the coefficients a_1, a_2, b_1 and b_2 , with two conditions where we can pick arbitrarily any a_1 and b_1 to specify some a_2 and b_2 ; the easiest election is $a_1 = b_1 = 0$, so $a_2 = b_2 = \frac{2\rho^3}{\nu}$.

The complete solution of eq. (5) is the sum of an homogenous and a particular solution. But homogenous solution can be multiplied by an arbitrary constant, that for simplicity we select to be zero.

$$\begin{bmatrix} u_1 \\ v_1 \end{bmatrix} = ik_c \begin{bmatrix} 0 \\ 2\rho^3/\nu \end{bmatrix} \left[(\partial_X B_X) e^{ik_c x} + (\partial_Y B_Y) e^{ik_c y} \right] + \text{c.c.} \quad (17)$$

Now with $\begin{bmatrix} u_0 \\ v_0 \end{bmatrix}$ and $\begin{bmatrix} u_1 \\ v_1 \end{bmatrix}$ we have all the information needed to get an explicit expression of $|R_2\rangle$. One we have $|R_2\rangle$ we can impose the solvability conditions and from them we will get equations

of the amplitudes B_H , B_X and B_Y .

Recalling (9) and (6), we have:

$$\begin{aligned}
|R_2\rangle &= -2(\partial_X\partial_x + \partial_Y\partial_y) \begin{bmatrix} 1 & -\alpha \\ \alpha & 1 \end{bmatrix} \begin{bmatrix} u_1 \\ v_1 \end{bmatrix} \\
&\quad - \begin{bmatrix} 1 + \tilde{d} + \nabla_{[X,Y]}^2 - \partial_t & -\alpha\nabla_{[X,Y]}^2 \\ \alpha\nabla_{[X,Y]}^2 & 1 - \tilde{d} + \nabla_{[X,Y]}^2 - \partial_t \end{bmatrix} \begin{bmatrix} u_0 \\ v_0 \end{bmatrix} \\
&\quad + (u_0^2 + v_0^2) \begin{bmatrix} 1 & -\beta \\ \beta & 1 \end{bmatrix} \begin{bmatrix} u_0 \\ v_0 \end{bmatrix}.
\end{aligned} \tag{18}$$

u_0 and v_0 are linear combinations of $\{e^{\pm i\omega_c t}, e^{\pm ik_c x}, e^{\pm ik_c y}\}$. Because of the terms $(u_0^2 + v_0^2)u_0$ and $(u_0^2 + v_0^2)v_0$, elements of $|R_2\rangle$ are going to be linear combinations of triple products $\{e^{\pm ia} \cdot e^{\pm ib} \cdot e^{\pm ic}\}$, where a , b and c takes all the possible values within the set $\{\omega_c t, k_c x, k_c y\}$, that is, linear combination of all cubic terms (pure and cross-terms).

As we are interested solely in the solvability condition which corresponds to $|R_2\rangle$, we do not need to obtain the complete expression of $|R_2\rangle$, but only the first order trigonometric polynomial terms, which are proportional to $e^{i\omega_c t}$, $e^{ik_c x}$ and $e^{ik_c y}$. It is not trivial that these terms of $|R_2\rangle$ belong to the image of \mathcal{M} , since the image is spanned by the vectors presented in (15), so we need to impose that condition.

Thus, let's now only present the $e^{i\omega_c t}$, $e^{ik_c x}$ and $e^{ik_c y}$ terms:

$$\begin{aligned}
(u_0^2 + v_0^2) u_0 &= [\Phi_{tU}] e^{i\omega_c t} + [\Phi_{xU}] e^{ik_c x} + [\Phi_{yU}] e^{ik_c y} \\
&\quad + [\Phi_{tU}^*] e^{-i\omega_c t} + [\Phi_{xU}^*] e^{-ik_c x} + [\Phi_{yU}^*] e^{-ik_c y} \\
&\quad + \text{the other cubic terms,}
\end{aligned} \tag{19}$$

and

$$\begin{aligned}
(u_0^2 + v_0^2) v_0 &= [\Phi_{tV}] e^{i\omega_c t} + [\Phi_{xV}] e^{ik_c x} + [\Phi_{yV}] e^{ik_c y} \\
&\quad + [\Phi_{tV}^*] e^{-i\omega_c t} + [\Phi_{xV}^*] e^{-ik_c x} + [\Phi_{yV}^*] e^{-ik_c y} \\
&\quad + \text{the other cubic terms,}
\end{aligned} \tag{20}$$

where

$$\Phi_{tU} \equiv (4c + 2/\rho)|B_H|^2 B_H + 4\eta(\eta c + 1)B_H(|B_X|^2 + |B_Y|^2) + 2c(\eta^2 + 1)B_H(|B_X|^2 + |B_Y|^2) \tag{21}$$

$$\Phi_{xU} \equiv 4(2\eta + 1/\rho)|B_H|^2 B_X + 3\eta(\eta^2 + 1)|B_X|^2 B_X + 6\eta(\eta^2 + 1)|B_Y|^2 B_X, \tag{22}$$

$$\Phi_{yU} \equiv 4(2\eta + 1/\rho)|B_H|^2 B_Y + 3\eta(\eta^2 + 1)|B_Y|^2 B_Y + 6\eta(\eta^2 + 1)|B_X|^2 B_Y. \tag{23}$$

$$\Phi_{tV} \equiv (4 + 2c/\rho)|B_H|^2 B_H + 4(\eta c + 1)B_H(|B_X|^2 + |B_Y|^2) + 2(\eta^2 + 1)B_H(|B_X|^2 + |B_Y|^2) \quad (24)$$

$$\Phi_{xV} \equiv 4(\eta/\rho + 2)|B_H|^2 B_X + 3(\eta^2 + 1)|B_X|^2 B_X + 6(\eta^2 + 1)|B_Y|^2 B_X, \quad (25)$$

$$\Phi_{yV} \equiv 4(\eta/\rho + 2)|B_H|^2 B_Y + 3(\eta^2 + 1)|B_Y|^2 B_Y + 6(\eta^2 + 1)|B_X|^2 B_Y. \quad (26)$$

.2 Solvability conditions

Let's show explicit expression of each term of $|R_2\rangle$, in left side of (9). In particular, we want to get a expression with the form:

$$\begin{aligned} |R_2\rangle &= |\Psi_t\rangle e^{i\omega_c t} + |\Psi_x\rangle e^{ik_c x} + |\Psi_y\rangle e^{ik_c y} + \text{c.c.} \\ &+ \text{the rest of pure and cross-cubic terms.} \end{aligned} \quad (27)$$

Once we get the explicit expressions of $|\Psi_t\rangle$, $|\Psi_x\rangle$ and $|\Psi_y\rangle$, we have to apply the solvability conditions:

$$\langle h_t | \Psi_t \rangle = 0, \quad (28a)$$

$$\langle h_x | \Psi_x \rangle = 0, \quad (28b)$$

$$\langle h_y | \Psi_y \rangle = 0, \quad (28c)$$

to make sure that the get the terms $|\Psi_t\rangle e^{i\omega_c t}$, $|\Psi_x\rangle e^{ik_c x}$ and $|\Psi_y\rangle e^{ik_c y}$ belong to the image of \mathcal{M} . From the three conditions (28) we will be obtain the amplitude equations for $B_H(X, Y, T)$, $B_X(X, Y, T)$ and $B_Y(X, Y, T)$.

We can continue to develop each term of right side of eq. (18), until we get $|R_2\rangle$ as a polynomial trigonometric series :

$$\begin{aligned} -\mathcal{L}_1 \begin{bmatrix} u_1 \\ v_1 \end{bmatrix} &= 4\alpha\rho(\partial_X^2 B_X) \begin{bmatrix} -\alpha \\ 1 \end{bmatrix} e^{ik_c x} \\ &+ 4\alpha\rho(\partial_Y^2 B_Y) \begin{bmatrix} -\alpha \\ 1 \end{bmatrix} e^{ik_c y} + \text{c.c.} \\ \\ -\mathcal{L}_0 \begin{bmatrix} u_0 \\ v_0 \end{bmatrix} &= \begin{bmatrix} -c(1 + \tilde{d})B_H + c\partial_T B_H - (c - \alpha)\nabla_{[X,Y]}^2 B_H \\ -(1 - \tilde{d})B_H + \partial_T B_H - (\alpha c + 1)\nabla_{[X,Y]}^2 B_H \end{bmatrix} e^{i\omega_c t} \\ &+ \begin{bmatrix} -\eta(1 + \tilde{d})B_X + \eta\partial_T B_X - \rho\nabla_{[X,Y]}^2 B_X \\ -(1 - \tilde{d})B_X + \partial_T B_X - (\alpha\eta + 1)\nabla_{[X,Y]}^2 B_X \end{bmatrix} e^{ik_c x} \\ &+ \begin{bmatrix} -\eta(1 + \tilde{d})B_Y + \eta\partial_T B_Y - \rho\nabla_{[X,Y]}^2 B_Y \\ -(1 - \tilde{d})B_Y + \partial_T B_Y - (\alpha\eta + 1)\nabla_{[X,Y]}^2 B_Y \end{bmatrix} e^{ik_c y} + \text{c.c.} \end{aligned}$$

$$\mathcal{N}_0 \begin{bmatrix} u_0 \\ v_0 \end{bmatrix} = \begin{bmatrix} (u_0^2 + v_0^2)u_0 - \beta(u_0^2 + v_0^2)v_0 \\ \beta(u_0^2 + v_0^2)u_0 + (u_0^2 + v_0^2)v_0 \end{bmatrix}.$$

Let's present each element separately. Reminding the outcome of $(u_0^2 + v_0^2)u_0$ and $(u_0^2 + v_0^2)v_0$ in (19,20):

$$(u_0^2 + v_0^2)u_0 - \beta(u_0^2 + v_0^2)v_0 = [\Phi_{tU} - \beta\Phi_{tV}]e^{i\omega_c t} + [\Phi_{xU} - \beta\Phi_{xV}]e^{ik_c x} + [\Phi_{yU} - \beta\Phi_{yV}]e^{ik_c y} + \text{c.c.} + \text{other cubic terms.}$$

$$\beta(u_0^2 + v_0^2)u_0 + (u_0^2 + v_0^2)v_0 = [\beta\Phi_{tU} + \Phi_{tV}]e^{i\omega_c t} + [\beta\Phi_{xU} + \Phi_{xV}]e^{ik_c x} + [\beta\Phi_{yU} + \Phi_{yV}]e^{ik_c y} + \text{c.c.} + \text{other cubic terms.}$$

Now that we have explicit expressions of the vectors $|\Psi_t\rangle$, $|\Psi_x\rangle$ and $|\Psi_y\rangle$ we can apply the solvability conditions (28) each of which will provide us an equation for the amplitudes B_H , B_X and B_Y , respectively.

Calculating inner product in eq. (28a), gives:

$$\begin{aligned} 0 = \langle h_t | \Psi_t \rangle &= \begin{bmatrix} -c^* \\ 1 \end{bmatrix}^\dagger \begin{bmatrix} -c(1 + \tilde{d})B_H + c\partial_T B_H - (c - \alpha)\nabla_{[X,Y]}^2 B_H \\ -(1 - \tilde{d})B_H + \partial_T B_H - (\alpha c + 1)\nabla_{[X,Y]}^2 B_H \end{bmatrix} \\ &+ \begin{bmatrix} -c^* \\ 1 \end{bmatrix}^\dagger \begin{bmatrix} \Phi_{tU} - \beta\Phi_{tV} \\ \beta\Phi_{tU} + \Phi_{tV} \end{bmatrix}, \\ 0 &= (c^2 - 1)B_H + (c^2 + 1)\tilde{d}B_H - (c^2 - 1)\partial_T B_H + (c^2 - 2\alpha c - 1)\nabla^2 B_H \\ &+ \left\{ -c \left[4(c - \beta) + \frac{2}{\rho}(1 - \beta c) \right] + \left[4(\beta c + 1) + \frac{2}{\rho}(\beta + c) \right] \right\} |B_H|^2 B_H \\ &+ \left\{ 4(\eta c + 1) [(\beta \eta + 1) - c(\eta - \beta)] + 4\rho \eta [(\beta c + 1) - c(c - \beta)] \right\} B_H (|B_X|^2 + |B_Y|^2), \end{aligned}$$

simplifying and using algebra results in (41), (42) and (44), with a_1 and a_2 defined in (35), finally we obtain the first amplitude equation:

$$\partial_T B_H = \left(1 - \frac{i}{\alpha} \tilde{d} \right) B_H + (1 + i\rho) \nabla^2 B_H - (4 + ia_1) |B_H|^2 B_H - (8\rho\eta + ia_2) B_H (|B_X|^2 + |B_Y|^2). \quad (29)$$

Continuing with eq. (28b):

$$0 = \langle h_x | \Psi_x \rangle = 4\alpha\rho(\partial_X^2 B_X) \begin{bmatrix} 1 \\ \alpha - \rho \end{bmatrix}^\dagger \begin{bmatrix} -\alpha \\ 1 \end{bmatrix} + \begin{bmatrix} 1 \\ \alpha - \rho \end{bmatrix}^\dagger \begin{bmatrix} -\eta(1 + \tilde{d})B_X + \eta\partial_T B_X - \rho\nabla_{[X,Y]}^2 B_X \\ -(1 - \tilde{d})B_X + \partial_T B_X - (\alpha\eta + 1)\nabla_{[X,Y]}^2 B_X \end{bmatrix} \\ + \begin{bmatrix} 1 \\ \alpha - \rho \end{bmatrix}^\dagger \begin{bmatrix} \beta\Phi_{xU} + \Phi_{xV} \\ \beta\Phi_{xU} + \Phi_{xV} \end{bmatrix},$$

$$0 = -4\alpha\rho^2(\partial_X^2 B_X) - 2(\alpha + \rho\tilde{d})B_X + 2\alpha\partial_T B_X + [-\rho - (\alpha - \rho)(\alpha\eta + 1)]\nabla_{[X,Y]}^2 B_X \\ + \left\{ 4\left[2(\eta - \beta) + \frac{1}{\rho}(1 - \beta\eta)\right] + 4(\alpha - \rho)\left[2(\beta\eta + 1) + \frac{1}{\rho}(\beta + \eta)\right] \right\} |B_H|^2 B_X \\ + 3\left[(\eta - \beta) + (\alpha - \rho)(\beta\eta + 1)\right](\eta^2 + 1) (|B_X|^2 + 2|B_Y|^2) B_X,$$

taking into account some algebra identities (36, 40, 46, 45), we have

$$\partial_T B_X = 2\rho^2(\partial_X^2 B_X) + \left(1 + \frac{\rho}{\alpha}\tilde{d}\right)B_X - 4\left(2 - 3\frac{\beta}{\alpha}\right)|B_H|^2 B_X - 6\rho\eta\left(1 - \frac{\beta}{\alpha}\right) (|B_X|^2 + 2|B_Y|^2) B_X. \quad (30)$$

The condition that comes from $\langle h_y | \Psi_y \rangle = 0$, eq. (28b), is simliar that the previous one obtained for $\langle h_x | \Psi_x \rangle = 0$. Due to the symmetry, it can be deduced the third amplitude equation for the evolution of B_Y ; this third equation will preserve the form of eq. (30) but exchanging B_x by B_y .

But we wish to have equations that do not depend in slow variables but only in terms of the regular ones, and we have to rescale. If $A(x, y, t)$ were the rescaled amplitude, it means that:

$$A(x, y, t) = \mu^{1/2} B(\sqrt{\mu}x, \sqrt{\mu}y, \mu t). \quad (31)$$

After rescaling the three equations: eq. (29) for Hopf amplitude H , (30) for x Turing amplitude T_{\parallel} and the corresponding eq. for y Turing amplitude T_{\perp} , the amplitude equations are obtained;

$$\frac{\partial H}{\partial t} = \left(\mu - \frac{i}{\alpha}d\right)H + (1 + i\rho)\nabla^2 H - (4 + ia_1)|H|^2 H - (8\rho\eta + ia_2)(|T_{\parallel}|^2 + |T_{\perp}|^2)H, \quad (32)$$

$$\frac{\partial T_{\parallel}}{\partial t} = \left(\mu + \frac{\rho}{\alpha}d\right)T_{\parallel} + 2\rho^2 \frac{\partial^2 T_{\parallel}}{\partial x^2} - 4\left(2 - 3\frac{\beta}{\alpha}\right)|H|^2 T_{\parallel} - 6\rho\eta\left(1 - \frac{\beta}{\alpha}\right) (|T_{\parallel}|^2 + 2|T_{\perp}|^2)T_{\parallel}, \quad (33)$$

$$\frac{\partial T_{\perp}}{\partial t} = \left(\mu + \frac{\rho}{\alpha}d\right)T_{\perp} + 2\rho^2 \frac{\partial^2 T_{\perp}}{\partial y^2} - 4\left(2 - 3\frac{\beta}{\alpha}\right)|H|^2 T_{\perp} - 6\rho\eta\left(1 - \frac{\beta}{\alpha}\right) (2|T_{\parallel}|^2 + |T_{\perp}|^2)T_{\perp}, \quad (34)$$

where

$$a_1 = \frac{2\beta}{\alpha\rho}(2\rho^2 + 1), \quad a_2 = \frac{4\beta}{\alpha}[2\alpha\rho(\alpha + \rho) + 3\rho + \alpha] - 4\eta. \quad (35)$$

.3 Useful identities and some algebra simplifications

$$\eta^2 + 1 = 2(\alpha\eta + 1) = 2\rho\eta \quad (36)$$

$$1/c = c^*, \quad \rightarrow \quad |c|^2 = c c^* = 1. \quad (37)$$

$$c^2 - 1 = \frac{2\alpha i}{\rho} c, \quad (38)$$

$$\frac{1}{c^2 - 1} = -\frac{\rho}{2\alpha} c^* i \quad (39)$$

$$-\rho - (\alpha - \rho)(\alpha\eta + 1) = 0 \quad (40)$$

$$1 - i\frac{\rho}{\alpha} c^* = -\frac{i}{\alpha}. \quad (41)$$

$$\begin{aligned} & \left(\frac{\rho}{2\alpha} c^* i \right) \left\{ c \left[4(c - \beta) + \frac{2}{\rho} (1 - \beta c) \right] - \left[4(\beta c + 1) + \frac{2}{\rho} (\beta + c) \right] \right\} \\ &= -(4 + ia_1). \end{aligned} \quad (42)$$

$$2(2\eta + 3\rho + 2\alpha\rho\eta + \rho\eta^2) = 4[\alpha + 3\rho + 2\alpha\rho(\alpha + \rho)]. \quad (43)$$

Result (43) is useful to do the following simplification:

$$\begin{aligned} & -\frac{\rho}{2\alpha} c^* i \left\{ 4(\eta c + 1) [(\beta\eta + 1) - c(\eta - \beta)] + 4\rho\eta [(\beta c + 1) - c(c - \beta)] \right\} \\ &= -(8\rho\eta + ia_2). \end{aligned} \quad (44)$$

$$\begin{aligned} & 2(\eta - \beta) + \frac{1}{\rho}(1 - \beta\eta) + (\alpha - \rho) \left[2(\beta\eta + 1) + \frac{1}{\rho}(\beta + \eta) \right] \\ &= 4\alpha - 6\beta. \end{aligned} \quad (45)$$

$$(\eta - \beta) + (\alpha - \rho)(\beta\eta + 1) = 2(\alpha - \beta). \quad (46)$$

Bibliography

- [BAC⁺00] D. Blair, I. S. Aranson, G. W. Crabtree, V. Vinokur, L. S. Tsimring, and C. Josserand. Patterns in thin vibrated granular layers: Interfaces, hexagons, and superoscillons. *Phys. Rev. E*, 61(5):5600–5610, 2000. [57](#)
- [Bal15] Philip Ball. Forging patterns and making waves from biology to geology: a commentary on turing (1952) ‘the chemical basis of morphogenesis’. *Philosophical Transactions B*, 2015. [14](#)
- [BDDW⁺02] Pierre Borckmans, Guy Dewel, Anne De Wit, Etiennette Dulos, Jacques Boissonade, Fabienne Gauffre, and Patrick De Kepper. Diffusive instabilities and chemical reactions. *International Journal of Bifurcation and Chaos*, 12(11):2307–2332, 2002. [12](#)
- [Bha07] A Bhattacharyay. A theory for one-dimensional asynchronous chemical waves. *J. Phys. A: Math. Theor.*, 40:3721–3728, 2007. [12](#), [40](#), [49](#)
- [BJP⁺95] P Borckmans, O Jensen, VO Pannbacker, E Mosekilde, G Dewel, and A De Wit. Localized turing and turing-hopf patterns. In *Modelling the Dynamics of Biological Systems*, pages 48–73. Springer, 1995. [12](#), [57](#)
- [Bon12] Laura Bones. How the cheetah gets its spots, 2012. [14](#)
- [BYK08] John Burke, Arik Yochelis, and Edgar Knobloch. Classification of spatially localized oscillations in periodically forced dissipative systems. *SIAM Journal on Applied Dynamical Systems*, 7(3):651–711, 2008. [38](#)
- [CE92] P. Couillet and K. Emilsson. Strong resonances of spatially distributed oscillators: a laboratory to study patterns and defects. *Physica D*, 61:119–131, 1992. [37](#), [38](#)
- [CH93] Mark C Cross and Pierre C Hohenberg. Pattern formation outside of equilibrium. *Reviews of Modern Physics*, 65(3):851, 1993. [12](#), [14](#), [19](#), [55](#)
- [CL90] P. Couillet and J. Lega. Breaking chirality in nonequilibrium systems. *Phys. Rev. Lett.*, 65:1352–1355, 1990. [38](#)
- [DBDW⁺95] Guy Dewel, Pierre Borckmans, Anne De Wit, B Rudovics, J-J Perraud, Etiennette Dulos, Jacques Boissonade, and Patrick De Kepper. Pattern selection and localized structures in reaction-diffusion systems. *Physica A: Statistical Mechanics and its Applications*, 213(1-2):181–198, 1995. [12](#), [40](#), [57](#)
- [DKBE90] Patrick De Kepper, J. Boissonade, and I. R. Epstein. Chlorite-iodide reaction: A ver-

- satellite system for the study of nonlinear dynamical behavior. *J. Phys. Chem.*, 94:6525–6536, 1990. [12](#), [40](#)
- [DKPBE94] Patrick De Kepper, J J Perraud, Rudovics B, and Dulos E. Experimental study of stationary turing patterns and their interaction with traveling waves in a chemical system. *Int. J. Bifurcation Chaos*, 4:1215–1231, 1994. [12](#), [20](#), [40](#), [43](#), [47](#), [57](#)
- [DW99] Anne De Wit. Spatial patterns and spatiotemporal dynamics in chemical systems. *Advances in Chemical Physics*, 109:435–514, 1999. [40](#)
- [DWLDB96] A. De Wit, D. Lima, G. Dewel, and P. Borckmans. Spatiotemporal dynamics near a codimension-two point. *Phys. Rev. E*, 54:261–271, 1996. [12](#), [40](#), [49](#)
- [EHM99] Christian Elphick, Aric Hagberg, and Ehud Meron. Multiphase patterns in periodically forced oscillatory systems. *Physical Review E*, 59(5):5285, 1999. [37](#)
- [EIT87] C Elphick, G Iooss, and E Tirapegui. Normal form reduction for time-periodically driven differential equations. *Physics Letters A*, 120(9):459–463, 1987. [37](#)
- [ES96] Iring R Epstein and Kenneth Showalter. Nonlinear chemical dynamics: Oscillations, patterns, and chaos. *J. Phys. Chem.*, 100:13132–13147, 1996. [12](#), [20](#)
- [Gam85] Jean Marc Gambaudo. Perturbation of a hopf bifurcation by an external time-periodic forcing. *Journal of Differential Equations*, 57(2):172–199, 1985. [37](#)
- [GCOSM90] Damià Gomila, Pere Colet, Gian-Luca Opp, and Maxi San Miguel. Stable droplets and growth laws close to the modulational instability of a domain wall. *Phys. Rev. Lett.*, 87:194101–1–194101–4, 1990. [38](#)
- [IF06] E. M. Izhikevich and R. FitzHugh. FitzHugh-Nagumo model. *Scholarpedia*, 1(9):1349, 2006. revision #123664. [25](#)
- [JBB⁺01] W Just, M Bose, S Bose, H Engel, and E Schöll. Spatiotemporal dynamics near a supercritical turing-hopf bifurcation in a two-dimensional reaction-diffusion system. *Phys. Rev. E*, 64:026219–1–026219–12, 2001. [40](#)
- [JPM⁺94] O. Jensen, V. O. Pannbacker, E. Mosekilde, Dewel G., and P. Borckmans. Localized structures and front propagation in the lengyel-epstein model. *Phys. Rev. E*, 50:736, 1994. [12](#), [20](#), [40](#), [43](#), [47](#), [49](#), [57](#)
- [Kee76] James P Keener. Secondary bifurcation in nonlinear diffusion reaction equations. *Studies in Applied Mathematics*, 55(3):187–211, 1976. [40](#)
- [Kid80] Hideyuki Kidachi. On mode interactions in reaction diffusion equation with nearly degenerate bifurcations. *Progress of Theoretical Physics*, 63(4):1152–1169, 1980. [40](#)
- [KL06] W. Klen and F. Leyvraz. Crystalline nucleation in deeply quenched liquids. *Phys. Rev. Lett.*, 57:2845, 2006. [24](#)
- [KM10] Shigeru Kondo and Takashi Miura. Reaction-diffusion model as a framework for understanding biological pattern formation. *Science*, 329(5999):1616–1620, 2010. [12](#)
- [Knu99] Carsten Knudsen. Frequency locking in forced oscillators, 1999. [37](#)
- [KS98] J. Keener and J. Sneyd. *Mathematical Physiology*. Springer-Verlag, New York, 1998. [12](#)

- [LHMS04] Anna L Lin, Aric Hagberg, Ehud Meron, and Harry L Swinney. Resonance tongues and patterns in periodically forced reaction-diffusion systems. *Phys. Rev. E*, 69(066217):1539–3755, 2004. [37](#)
- [MCY17] Paulino Monroy Castellero and Arik Yochelis. Comb-like turing patterns embedded in hopf oscillations: Spatially localized states outside the 2:1 frequency locked region. *Chaos*, 27:043110–1–043110–8, 2017. [11](#), [47](#)
- [Mer15] Ehud Meron. *Nonlinear Physics of Ecosystems*. CRC Press, 2015. [11](#), [12](#), [13](#), [14](#), [24](#), [37](#), [39](#), [55](#)
- [MHM09] Yair Mau, Aric Hagberg, and Ehud Meron. Dual-mode spiral vortices. *Phys. Rev. E*, 80:065203–1–065203–4, 2009. [12](#), [49](#)
- [MPC97] Philip Maini, Kevin Painter, and Helene Nguyen Phong Chau. Spatial pattern formation in chemical and biological systems. *Journal of the Chemical Society, Faraday Transactions*, 93(20):3601–3610, 1997. [12](#)
- [Mur02] J. D. Murray. *Mathematical Biology*. Springer, New York, 2002. [12](#)
- [Oel14] Thomas Oelmann. more cloud stripes, 2014. [14](#)
- [OGB98] M Or-Guil and M Bode. Propagation of turing-hopf fronts. *Physica A*, 249:174–178, 1998. [41](#)
- [PDWD⁺93] J-J Perraud, Anne De Wit, Etiennette Dulos, Patrick De Kepper, Guy Dewel, and Pierre Borckmans. One-dimensional “spirals”: Novel asynchronous chemical wave sources. *Physical Review Letters*, 71(8):1272, 1993. [12](#), [43](#), [49](#)
- [Pis06] L. M. Pismen. *Patterns and Interfaces in Dissipative Dynamics*. Springer-Verlag, Berlin, 2006. [12](#)
- [PR07] A. Pikovsky and M. Rosenblum. Synchronization. *Scholarpedia*, 2(12):1459, 2007. revision #128276. [37](#)
- [SCT⁺12] István Szalai, Daniel Cuiñas, Nándor Takács, Judit Horváth, and Patrick De Kepper. Chemical morphogenesis: recent experimental advances in reaction–diffusion system design and control. *Interface Focus*, 2(4):417–432, 2012. [12](#)
- [Ste08] Peter S. Stevens. *Entropy and the Time Evolution of Macroscopic Systems*. Oxford Science Publications, 2008. [13](#)
- [Ste15] Peter S. Stevens. *Patterns in nature*. An Atlantic Monthly Press book, 2015. [13](#)
- [TMB⁺13] J C Tzou, Y P Ma, A Bayliss, B J Matkowsky, and V A Volpert. Homoclinic snaking near a codimension-two turing-hopf bifurcation point in the brusselator model. *Phys. Rev. E*, 87:022908–1–022908–20, 2013. [12](#), [39](#), [41](#), [44](#), [56](#)
- [Tur52] Alan M. Turing. The chemical basis of morphogenesis. *Philosophical Transactions of the Royal Society of London. Series B, Biological Sciences*, 237:37–72, 1952. [14](#)
- [VE08] Vladimir K Vanag and Irving R Epstein. Design and control of patterns in reaction-diffusion systems. *Chaos*, 18(2):026107, 2008. [12](#), [57](#)
- [VE09] Vladimir K Vanag and Irving R Epstein. Cross-diffusion and pattern formation in

- reaction–diffusion systems. *Physical Chemistry Chemical Physics*, 11(6):897–912, 2009. [30](#)
- [VP09] V Volpert and S Petrovskii. Reaction–diffusion waves in biology. *Physics of Life Reviews*, 6(4):267–310, 2009. [12](#)
- [Wik17] Wikipedia. Patterned vegetation — wikipedia, the free encyclopedia, 2017. [Online; accessed 30-May-2017]. [14](#)
- [YEHM04a] Arik Yochelis, Christian Elphick, Aric Hagberg, and Ehud Meron. Frequency locking in extended systems: The impact of a turing mode. *EPL*, 69:170, 2004. [41](#)
- [YEHM04b] Arik Yochelis, Christian Elphick, Aric Hagberg, and Ehud Meron. Two-phase resonant patterns in forced oscillatory systems: boundaries, mechanisms and forms. *Physica D*, 199:201–222, 2004. [38](#), [41](#), [42](#), [45](#), [48](#), [51](#), [53](#), [55](#)
- [YHM⁺02] Arik Yochelis, Aric Hagberg, Ehud Meron, Anna L Lin, and Harry L Swinney. Development of standing-wave labyrinthine patterns. *Siam J. Applied Dynamical Systems*, 1:236–247, 2002. [38](#), [40](#), [41](#), [48](#), [56](#), [57](#)